Rita Bagaine Kagoro

The effect of surfactant type, velocity and permeability on CO_2 foam under miscible conditions

TU Delft

The effect of surfactant type, velocity and permeability on CO_2 foam under miscible conditions

By

Rita Bagaine Kagoro

in partial fulfilment of the requirements for the degree of

Master of Science
in Applied Earth Sciences

at the Delft University of Technology,
to be defended publicly on Tuesday August 29, 2017 at 2:00 PM.

Student Number	4466810

Supervisor:

Dr. R. Farajzadeh	Delft University of Technology, Shell Global Solutions B.V.

Thesis committee:

Prof. Dr. W. R. Rossen	Delft University of Technology
Prof. Dr. K.H.A.A. Wolf	Delft University of Technology
Prof. Dr. J. Bruining	Delft University of Technology
Dr. S. Vincent Bonnieu	Shell Global Solutions B.V.
Dr. S. Kahrobaei	Delft University of Technology

TU Delft

Abstract

Miscible gas injection has been widely used worldwide to improve oil recovery. However, problems such as viscous fingering and gravity override undermine its success on a large scale. Foaming of the injected gas mitigates these problems by reducing the mobility of the gas.

Past studies using an ionic surfactant to foam CO_2 in the presence of decane discovered the presence of three distinct regions based on the fraction of CO_2 in the CO_2-decane mixture namely; CO_2-rich floods where the apparent viscosity increased with the increase in the CO_2 molar fraction, decane-rich floods where the apparent viscosity decreased with the increase in the CO_2 molar fraction and floods with intermediate CO_2 molar fraction where the apparent viscosity was independent of the CO_2 molar fraction in the CO_2-decane mixture. The foam quality scans showed that the CO_2-rich floods and decane-rich floods exhibited both low and high-quality regimes while the floods with intermediate CO_2 molar fractions lacked a high-quality regime [1].This behaviour was not fully understood.

The effect of the surfactant type on the observed behaviour has been studied in this thesis by using a non-ionic surfactant in the foam quality scans. The results show the presence of the three distinct regions as observed in the previous study with an ionic surfactant. However, this study shows that the quality scans of all the CO_2-decane molar compositions exhibit both the high and low-quality regimes. This study also shows that both the low and high-quality regimes are present at high flow rates. In addition, the flow behaviour is shear-thinning in nature and can be modelled by the power law.

Furthermore, the transient generation of CO_2 foam in the presence of decane at different CO_2-decane molar compositions has been investigated. The results show that the generation of CO_2 foam in the presence of decane depends on the injected amount of CO_2-decane mixture and is independent of the CO_2-decane molar composition and quality.

Lastly, the effect of permeability on transient foam generation has been tested in low permeability cores and has been compared to foam generation in high permeability cores. The results show that foam generation occurs earlier in low permeability cores. In addition, the low permeability cores are susceptible to damage and blockage especially at high injection rates.

Table of contents

1 Introduction

Worldwide energy demand has increased in recent years leading to a surge in research and development of Enhanced Oil recovery (EOR) methods. Moreover, this increase in demand, coupled with the maturation of several oil fields and fewer new discoveries worldwide, have created an interest in extracting additional oil from available fields [2]. After primary recovery, a significant amount of oil remains trapped due the capillary forces that exist between oil, water and the rock [3]. Considering this, several technologies have been developed to extract this remaining oil through enhanced oil recovery. Several successful EOR treatments have been based on the injection of gases into the reservoir.

1.1 Gas Injection

Gas injection is a process that introduces gases into the reservoir to produce additional oil [4]. There are two main processes of gas injection in practice namely; immiscible gas injection and miscible gas injection. The immiscible process results in two-phase flow and improves oil recovery through oil swelling and viscosity reduction. The miscible process allows the oil and gas to form one phase by reducing the interfacial tension between the oil and gas which increases the displacement efficiency, leading to incremental oil recovery [5]. However, both these processes face challenges such as viscous fingering [6], which allows the less viscous gas to form fingers that channel through the reservoir; heterogeneity [7], which creates thief zones that lead to early gas breakthrough and finally, gravity override [8], which causes the fluids to separate based on their densities, leaving the lower parts of the reservoir poorly swept.

The miscibility between gas and oil can be achieved in two ways namely; first contact miscibility (FCM), where oil and a gas form a single phase when mixed in any proportion at a given temperature and pressure, and multi contact miscibility (MCM), where the injected gas exchanges components with oil until a state of miscibility is achieved in the mixing zone [9]. There are two ways in which multi contact miscibility can be achieved namely; vaporizing drive and condensing drive. Vaporizing drive is where lighter and intermediate components from the oil phase enter the gas phase. The resulting mixture contacts “virgin” oil and mixes with more lighter components. This process continues until one phase is formed through “multiple contact” with oil [9]. During condensing drive, intermediate components from the gas phase enter the oil phase. The resulting mixture is contacted by “virgin” gas and more intermediate components are extracted until 1 phase is formed by multiple contact with injected gas [9].

1.2 Carbon dioxide flooding

Injecting gas under miscible conditions causes the capillary and interfacial forces to vanish [10]. CO_2 is therefore a prime candidate for injection as a miscible gas. This is because it has a low minimum miscibility pressure (MMP) [5], which can be achieved in many reservoirs. MMP is the lowest pressure at a given temperature where miscibility can be achieved between a reservoir fluid and the injected gas [9].

The MMP of Carbon dioxide can be determined through the slim tube experiment as well as core floods [1]. At a constant temperature, experiments in which CO_2 displaces oil are carried out at different pressures. The oil recovery at 1.2 PV is recorded for these experiments. The oil recovery is plotted against the pressure and a kink in the graph is observed where the gradient of the line changes. (see

Figure 1.1). This point is noted as the MMP. Below this point, the drive is immiscible while above this point, the drive is developed miscibility for an oil with multiple components and first contact miscibility for an oil with one component.

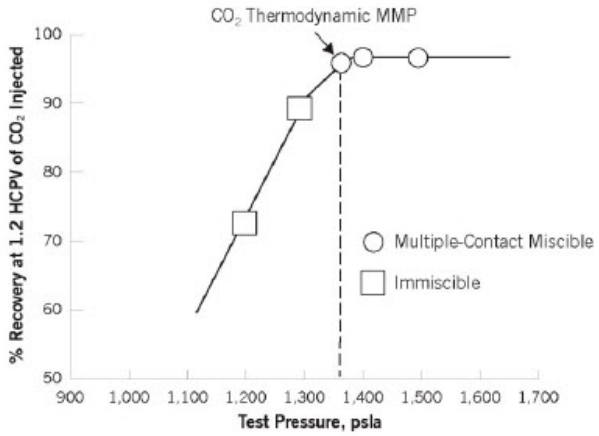

Figure 1.1: Results of a slim tube experiment to determine the MMP. [11]

The main causes of low oil recovery using CO_2 gas on a large scale are the density and viscosity of the gas. The low density promotes gravity override, which reduces oil recovery in the lower portions of the reservoir while the low viscosity results in an unfavourable mobility ratio, which leads to viscous fingering and ultimately, early breakthrough of the injected gas [12].

1.2.1 The effect of supercritical CO_2 on decane

The pressure (90 bar) and temperature (40°C) conditions in this study mean that CO_2 is a supercritical fluid. It is therefore vital to understand how supercritical CO_2 affects the properties of decane.

When supercritical CO_2 is mixed with decane, it lowers the interfacial tension between decane and water. Low interfacial tension (IFT) reduces the capillary pressure and consequently, the pressure gradient required to mobilize oil through constrictions. A study by Liu et al. [13]. on the use of supercritical CO_2 in enhanced oil recovery showed that the IFT of water-CO_2-decane decreases linearly with the increase in molar fraction of CO_2.This is further supported by studies by Sun and Chen [14] and Georgiadis et al. [15].

When CO_2 molecules were solubilized in decane, they were found to reduce the IFT value by accumulating at the water-decane interface hence playing “surface active” at the interface. The CO_2 molecules however did not accumulate at the water-CO_2 interface in the absence of decane. Therefore, it was determined that the accumulation of CO_2 at the water-decane interface was driven by the IFT difference between CO_2-water and water-decane (The IFT of water-CO_2 is 18mN/m lower than that of water-decane) [13].

Furthermore, physical properties such as the density and viscosity of decane are affected by addition of supercritical CO_2 to the system. Figure 1.2 shows the density and viscosity of the CO_2-decane binary mixture as a function of the CO_2 molar fraction at the experimental conditions of this study. This data was calculated using the NIST Reference Fluid Thermodynamic and Transport Properties Database (REFPROP) [16].

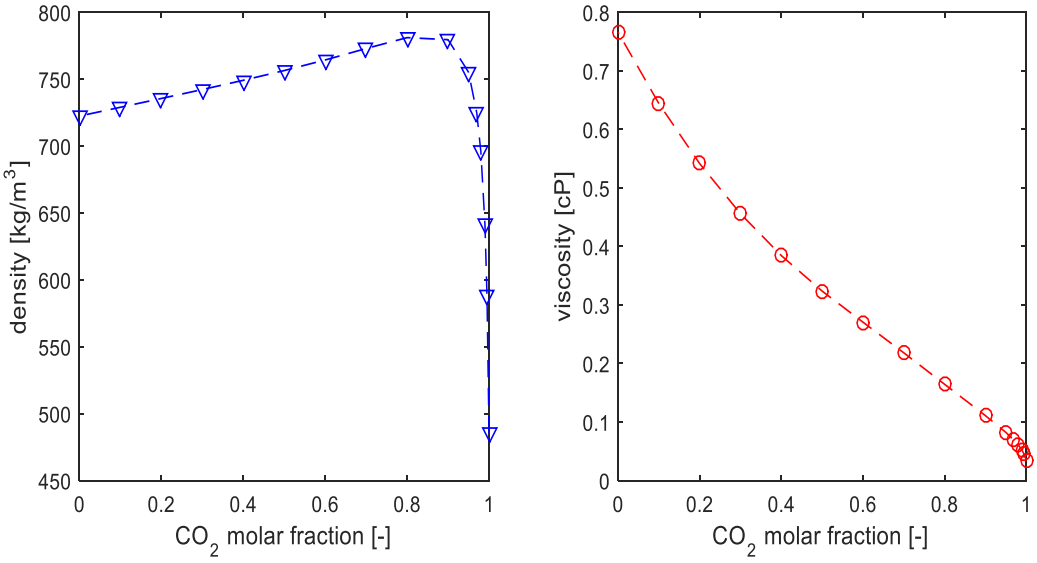

Figure 1.2: The density (left) and viscosity (right) of the CO_2-decane binary mixture as a function of CO_2 molar composition.

1.3 Foam as a mobility-control agent

Foam (Figure 1.3), is a two-phase medium of gas and liquid made up of gas pockets trapped in a network of thin liquid films (lamellae) and plateau borders [17].

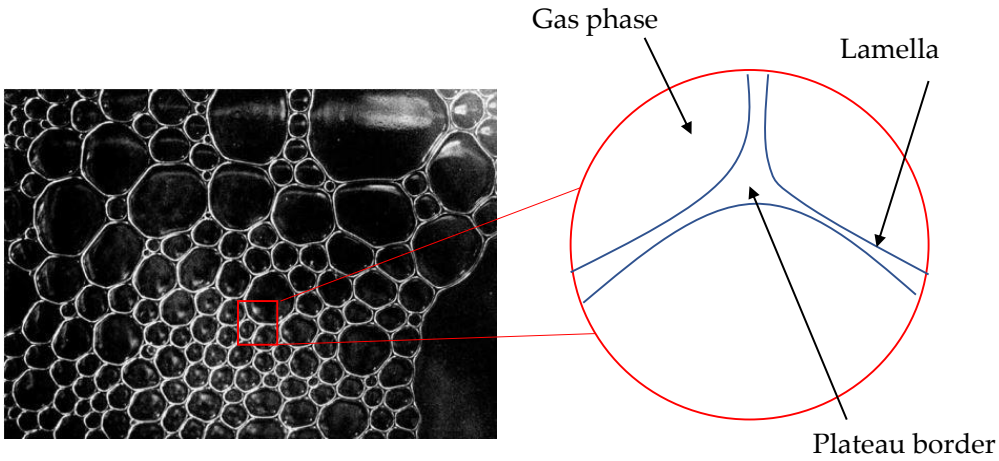

Figure 1.3: The structure of foam [18]

Foam as an EOR method arose out of the need to mitigate the problems associated with gas injection. It has been used to control gas mobility and improve sweep efficiency during gas injection by increasing the effective viscosity and decreasing the relative permeability of the injected gas [19].

1.3.1 The role of surfactants

To generate a stable foam, a surfactant is required. A surfactant is a compound that reduces the surface tension of the solvent or the interfacial tension between two non-miscible liquids [20]. A surfactant has a hydrophilic (water-soluble) component as well as a hydrophobic (oil-soluble) group made up of a hydrocarbon chain [21]. When a liquid is mixed with a gas in the presence of a surfactant, the surfactant molecules adsorb at the interface to create a foam. Surfactants create emulsions when immiscible liquids like water and oil are mixed. Above a critical surfactant concentration called the critical micelle concentration (CMC), surfactant molecules form aggregates called micelles (shown in Figure 1.4) [22].

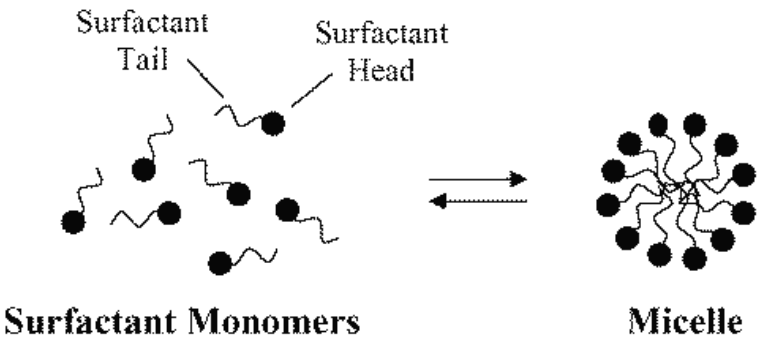

Figure 1.4: Micelle formation in surfactants. [23]

In aqueous solutions, micelles form with the polar head of the surfactant molecules on the micelles surface, extending out into the solvent. Reverse micelles form in non-polar solvents with the polar surfactant heads in the centre of the micelle and the hydrophobic surfactant tails extending into the organic solvent [24].

As the surfactant concentration in the solution increases, the surface tension reduces until the CMC is reached. Above this concentration, the surface tension remains constant. Generally, the amount of foam produced by a surfactant increases with concentration to a maximum at CMC [20]. Moreover, small bubbles form at mainly high surfactant concentrations while larger bubbles form at lower concentrations [25].

Prior to the field implementation of a foam treatment, surfactant screening experiments are necessary to determine the best surfactant type for specific reservoir conditions. Available surfactants are usually classified into two main groups namely; ionic surfactants and non-ionic surfactants [20]. Ionic surfactants dissociate in water into anions or cations for anionic and cationic types respectively. Surfactant molecules that exhibit both anionic and cationic dissociations are known as amphoteric or zwitterionic surfactants [21]. Non-ionic surfactants do not dissociate in aqueous solutions because their hydrophilic group is of a non-dissociable type [26].

Establishing a correlation between the foaming ability of a surfactant and its structure is a complex process. There is no concrete relationship between the structure of a surfactant and its foaming ability [20]. Some structural variations like the increase of the chain length of an alkyl sulphate can increase the surfactant's foaming ability. Adkins et al. [27]. found that increasing the length of the surfactant tail increases the efficiency of the surfactant at the air-water interface linearly as the tail becomes more hydrophobic. However, much longer chains lead to lower surfactant solubility and reduced diffusion [20].

Other structural variations like branching of the tail or moving the hydrophilic group to an internal position also affect foam generation. Surfactants with branched tails are more efficient than those with linear tails of the same length. On the other hand, they are less efficient than surfactants with linear tails of the same carbon number [28].

The ionic nature of the surfactant also affects foam generation [29]. Non-ionic surfactants for example have a larger surface area per molecule compared to ionic surfactants, making it difficult for the surfactant tails to interact laterally, resulting in a low interfacial elasticity [20]. The use of a non-ionic surfactant in this study gives us an insight into their behaviour when used for foam generation.

1.3.2 Foam Generation and propagation

There are three main mechanisms (shown in Figure 1.5), that lead to foam generation in porous media. These include; snap-off, leave-behind, and lamella division [19].

The snap-off mechanism describes the formation of bubbles when the gas pushes the gas-liquid interface through a pore throat causing the interface to snap off [30]. The leave-behind mechanism describes the formation of liquid lenses left behind when two gas bubbles enter a pore occupied by liquid [30]. This method dominates foam generation below a certain critical velocity [31], where weak foam is abruptly converted into strong foam. The division of lamella happens when existing foam bubbles are subdivided [30] as mobilized lamellae pass a pore body with more than one pore throat [32].

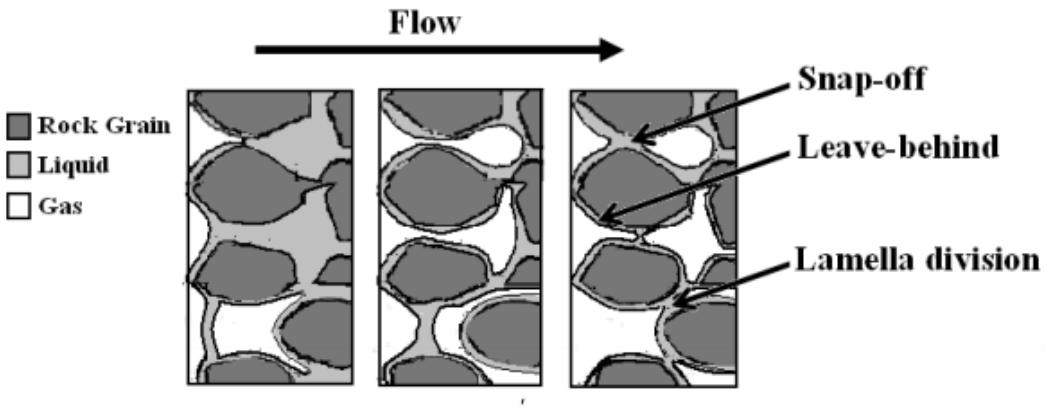

Figure 1.5: Mechanisms of foam generation in porous media [19].

During the flow of foam, bubble regeneration, coalescence and destruction may occur [25]. Bubbles form in the largest pores first and advance forward. This is due to the lower capillary entry pressure in larger pores compared to small ones. The pressure gradient then increases and bubbles start to invade smaller pores. As foam is generated, the pressure drop across the porous rock increases until a steady state is reached. At steady state, the rate of bubble generation and destruction is the same [31].

Some studies report a minimum pressure gradient or a critical injection velocity for generating foam [33, 34, 35]. Moreover, if the pressure gradient is not sufficient to mobilise lamellae, gas flow stops, and foam plugs the flow path [30]. Rossen argues that this pressure gradient depends on the fraction of pore throats blocked by snap off, which in turn depends on capillary pressure. When few throats are blocked, an

insufficient pressure gradient results, causing gas to flow as a continuous phase, resulting in lower mobility reduction [36].

Chou [37] carried out a set of experiments to determine the conditions for generating foam in porous media using different initial conditions of the core. He found that, foam was readily formed whenever the core was first pre-saturated with surfactant solution, regardless of flow rate or pressure gradient. Furthermore, in cases where foam was not readily created, increasing surfactant saturation in the core solved this issue.

The flow of foam has generally been described by two regimes namely; low and high-quality regimes. In the high-quality regime, the foam apparent viscosity decreases with increase in foam quality and the steady-state pressure gradient is independent of the gas flow rate. The foam apparent viscosity increases with foam quality in the low-quality regime and the pressure gradient is independent of liquid flow rate [30]. Foam quality is defined as the ratio of the gas volumetric flow rate to the total volumetric flow rate.

1.3.3 Foam Stability in porous media

Foams have been shown to be thermodynamically unstable [17, 38, 39]. They are subject to drainage, coarsening and eventually, they collapse when the films between the bubbles are ruptured [26, 40].

Foams maintain stability in different ways. A positive (disjoining) pressure is known to stabilize foam, while a negative (conjoining) pressure destabilizes it [38]. In general, the positive disjoining pressure arises from the effect of the repulsive electric double layer, where adsorption of ionic surfactant on the thin lamellae films causes the like charges on two nearby films to repel each other thus preventing thinning of the liquid films [41], while the negative pressure arises from attractive van der Waals forces [42].

When a liquid film is stretched, the surfactant concentration decreases in the stretched region which causes the surface tension to increase [43]. This increase in surface tension stops the stretching, and a new equilibrium is reached. This changing surface tension (elasticity) helps foams to maintain stability [44].

Foam film stability is significantly affected by gas diffusion through foam films. Diffusion occurs when the bubbles in a newly formed foam are of unequal size. The smaller bubbles have a higher internal pressure compared to the larger bubbles and therefore gas diffuses from the smaller bubbles to the larger ones, hence coarsening the foam [45, 46, 47].

The stability of foam in the presence of oil is one of the biggest concerns in the application of foam in oil reservoirs. For this EOR method to be effective, foam must maintain stability when it encounters oil [48]. When two adjacent thin liquid films approach each other past a critical thickness, the negative disjoining pressure becomes strong enough to rupture the films. Oil destabilizes foam in the same way; by changing the surface tension, which in turn allows liquid film thinning past the critical thickness [38].

This effect of oil on foam performance has been studied both under miscible [1] and immiscible conditions [49] with injected gas. Foam was found to be more unstable in the presence of intermediate oil components compared to heavier oil components (above C6) [50]. The collapse of foam was probably because of the smaller molecules of light components that might easily access the interface of gas and surfactant solution, consequently rupturing the lamella. The same observation was evident in experiments by Osei-Bonsu et al. [41] which showed that shorter chain hydrocarbons were more destabilising to foam films than longer chain hydrocarbons. On the other hand, some foams made from

surfactants with perfluorinated tails instead of hydrocarbon ones, were found to be the stable in the presence of lighter components of crude oil. [26].

Microfluidic experiments by Osei-Bonsu et al. [51] using pre-generated foam injected directly into an oil saturated model showed that lamellae generated by foam at qualities above 85% could not tolerate the effect of oil, which led to a less stable front and a reduced recovery factor. This was attributed to the thinner lamellae and smaller plateau borders produced at high gas fractional flows that are more susceptible to collapse due to oil invasion into the gas-liquid interface.

Foam stability, in the presence of oil droplets, is controlled by the stability of the film formed between the air-water interface and an approaching oil drop. Wasan et al. [52] termed this, a 'pseudoemulsion' film. Koczo et al. [49]. found that the effect of oil on foam stability and its mechanism depends on whether the oil is solubilized or emulsified and whether the pseudoemulsion film is stable or not. In the presence of emulsified oil, foam stability was found to increase if the pseudoemulsion film was stable [53]. The emulsified oil drops accumulated in the plateau borders, and hindered liquid drainage from the films.

Lee et al. [54] studied the stability of a single foam film containing swollen micelles of a non-ionic surfactant to understand the role of oil solubilized by micelles on foam stability. They found that the presence of n-dodecane swollen micelles, led to a lower film thickness and instead destabilized the foam.

Several foam core flooding experiments identify an abrupt shift from the low-quality regime to the high-quality regime [1, 55, 56], at a value of capillary pressure called the 'limiting capillary pressure' P_c^*. This occurs at the 'transition' foam quality, f_g^*. At the limiting capillary pressure, foam lamellae rapidly coalesce causing foam to collapse [57]. The limiting capillary pressure depends on the surfactant type and concentration, foam flow rate and permeability [56].

Lastly, core flooding experiments under miscible conditions using CO_2 gas and decane [1] revealed that CO_2-rich floods and decane-rich floods exhibited both the high and low-quality regimes while floods with intermediate CO_2-decane molar compositions only exhibited a low-quality regime when an ionic surfactant was used. This is behaviour was not fully understood and is thus the focus of this thesis.

1.3.4 Field Application of foam

A number of foam treatments have been implemented in several fields with positive results. Some field operations such as the mature Cuisiana field in Colombia, Salt Creek Field and the SACROC field in West Texas, realized decreased injectivity, incremental oil production and cuts in Gas-Oil ratios at production wells after implementing foam treatments.

These fields generally experienced increased well head pressure proving that foam reduces injectivity through gas blocking. In addition, oil flow rate increase and Gas-Oil ratio reductions were observed in the affected fields with some happening within two months after treatment [58].

The effects of foam application were also observed in the Snorre Field in the North Sea on the Norwegian continental shelf. The foam pilot utilised a hydrocarbon gas to generate foam which significantly delayed the breakthrough of gas at the production well, leading to an additional 250,000 Sm^3 of incremental oil [59].

Foam pilots in the East Vacuum Grayburg/San Andres Unit, the SACROC field in West Texas and in Salt Creek Field led to a 30% [60], 50% [61] and 40% reduction in gas injectivity respectively as well as delayed breakthrough of post foam tracer in the Salt Creek field. This was attributed to the mobilization

of reservoir liquids deep in the reservoir due to foam generation that stopped CO_2 from channelling through high conductivity pathways, hence improving overall sweep [62]. Strong foams that reduced CO_2 injectivity by 40% to 85% for up to 6 months were also generated using AOS (Chaser CD1040) in the North Ward-Estes field in Texas [63].

1.4 Emulsions

An emulsion is a metastable dispersion of one liquid in a second immiscible liquid. [64]. To stabilize an emulsion against coalescence, a surfactant or emulsifier should also be present. Two types of emulsions are readily defined in literature namely; water-in-oil emulsions and oil-in-water emulsions [53].

In a foam treatment in the presence of oil, emulsions may form when surfactant solution and oil come into contact especially at high shear rates. Emulsified oil occurs in two forms namely; solubilized within micelles (micro emulsions) and as macro emulsion drops [54].

1.4.1 Flow of macro emulsions in porous media

Just like foam, emulsions in porous media can also improve sweep efficiency. By flowing into large pores, they block high permeability zones and divert injected fluids to the less permeable parts of the reservoir [65, 66].

When emulsion droplets flow in porous media, they reduce the permeability in different ways. Macroemulsions plug pore throats of sizes smaller than their own by lodging between sand grains [67]. This occurs when the pressure gradient is not enough to deform the droplets through the constrictions in the flow path. When an emulsion droplet enters a narrow part of a pore throat, its radius of curvature at the foremost end becomes smaller than the radius of the part still in the pore. (shown in Figure 1.6). The capillary pressure at the front of the drop is thus greater than at the back, and an extra pressure gradient is required to push the droplet through. This “Jamin” effect increases as the droplets encounter more pore constrictions. As the retention of droplets increases, fluid flow is diverted to the larger pores where the chances of capture are lower. When droplet capture can no longer proceed, steady state is achieved [65].

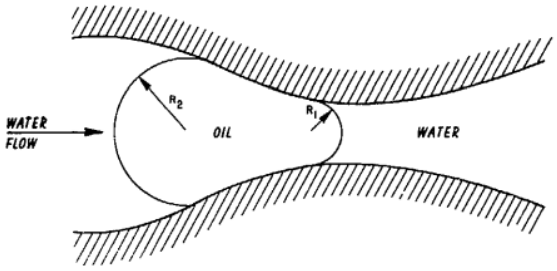

Figure 1.6: An oil droplet entering a pore constriction. [65]

Cobos et al. [68] also analysed the flow of oil-in-water emulsions through quartz micro-capillary tubes. They used capillaries as models of connecting pore-throats between adjacent pairs of pore bodies. The average oil drop size varied from smaller to larger than the neck radius. Oil drops that were larger than the constrictions were found to partially block the capillary tubes, leading to a high extra pressure difference at low capillary numbers [68].

The Capillary number, C_a is defined as;

$$C_a = \frac{\mu_c v}{\sigma} \quad (1.1)$$

Where;

v = Darcy velocity [m/s]

σ = interfacial tension between dispersed and continuous phase [N/m]

μ_c = effective viscosity of the continuous phase [Pa.s]

They also found that the pressure drop required to mobilize oil drops of sizes smaller than the capillary throat diameter did not vary with capillary number but was a function of the viscosity ratio, dispersed phase concentration and droplet size distribution.

Core flooding experiments by Romero also showed that the apparent viscosity of emulsions is a strong function of Capillary number. The observed partial pore blocking phenomenon was a strong function of the capillary number and the ratio of the size of the dispersed phase drops to the throat radius. For emulsions with very small drops (2μm) flowing through a high permeability network (901.6mD), a constant apparent viscosity was observed. There was no pore blocking and the flow behaviour was similar to that of the continuous phase. When drop sizes were increased from 10μm and 20μm, pore blocking was observed and the apparent viscosity fell with increasing capillary number and rose with increasing drop size in this region. Furthermore, the partial pore blocking mechanism occurred below a certain critical value of capillary number which was a function of the emulsion properties and the geometry of the pore space. To prevent pore plugging in porous media, the ratio of the average pore size to the mean emulsion droplet size should be high. The emulsion droplets in this case reduce permeability though adsorption on the pore surface which decreases the area available for flow [69].

Core flooding experiments by Uzoigwe and Marsden [70] showed that the apparent viscosity of emulsions increased with quality, with this increase being more noticeable at low shear rates (shown in Figure 1.7). In addition, qualities ≤50% were found to have Newtonian characteristics while qualities above 50% were shear-thinning. These experiments were carried out in high permeability unconsolidated and synthetic porous media.

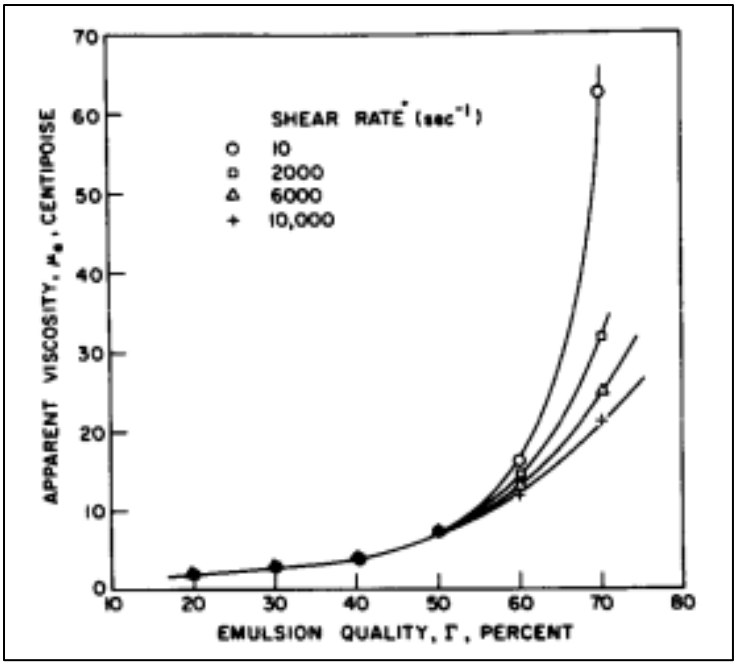

Figure 1.7: Emulsion apparent viscosity as a function of quality [70]

2 Scope of present study

The objective of this thesis is to gain more knowledge on the behaviour of supercritical CO_2 foam in the presence of decane under miscible conditions. The motivation for this thesis was derived from a previous study by Kahrobaei et al. [1] whose observations are briefly outlined below.

2.1 Motivation

Kahrobaei et al. [1] carried out CO_2 foam quality experiments with an ionic surfactant (Alpha Olefin Sulfonate (AOS) C14-17 (Stepan® BIO-TERGE AS-40 KSB)) at different CO_2-decane molar compositions to mimic the interaction gas and oil would have in the reservoir. The total flow rate was 1.6ml/min. The study showed that in the presence of oil, foam flow showed three distinct regions as the molar fraction of CO_2 in the CO_2-decane mixture was increased from 0 to 1 namely; CO_2-rich floods where the apparent viscosity increased with the increase in the CO_2 molar fraction, decane-rich floods where the apparent viscosity decreased with the increase in the CO_2 molar fraction and floods with intermediate CO_2 molar fraction where the apparent viscosity was independent of the CO_2 molar fraction in the CO_2-decane mixture (see Figure 2.2). The decane-rich and CO_2-rich quality scans exhibited both low and high-quality regimes while intermediate CO_2-decane molar compositions showed a constant apparent viscosity with increasing quality (shown in Figure 2.1). A quality scan is the measurement of the apparent viscosity of foam at different qualities.

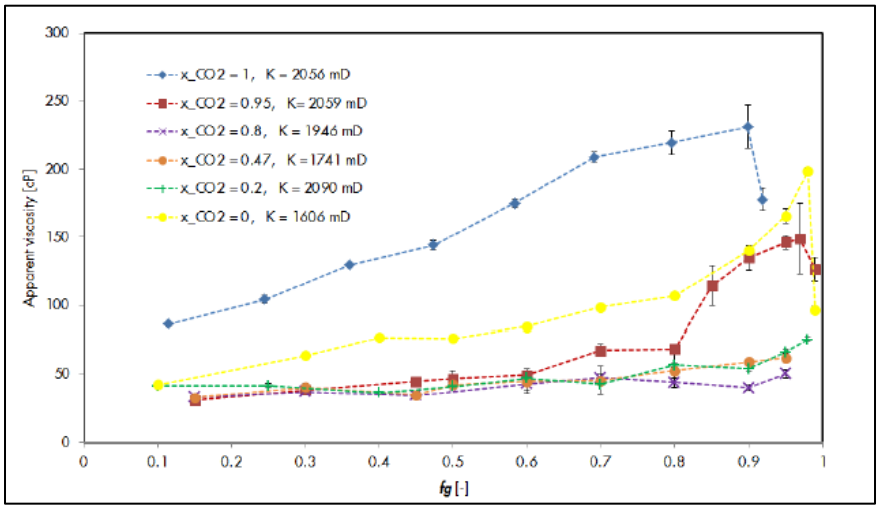

Figure 2.1:Foam apparent viscosity as a function of quality for different CO_2 molar fractions using AOS surfactant [1].

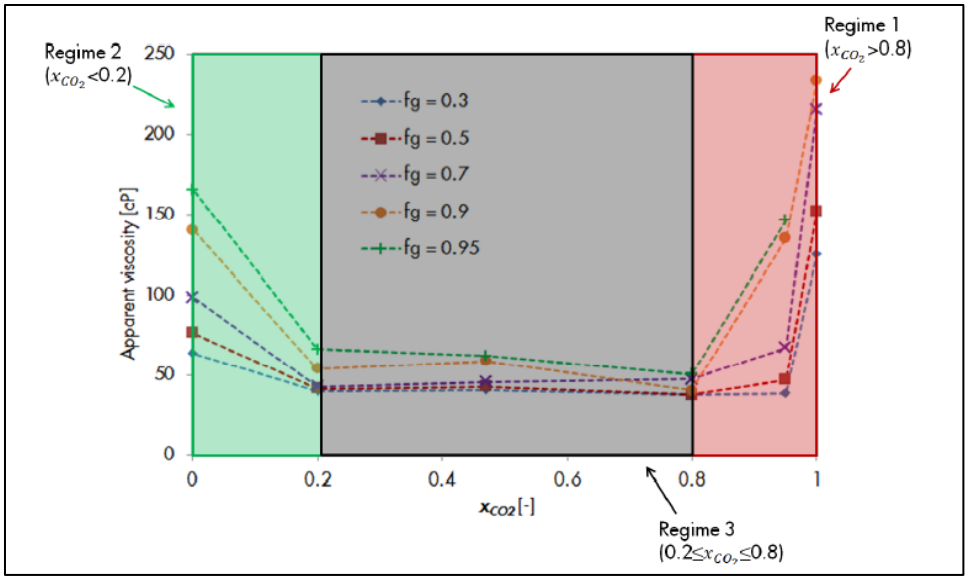

Figure 2.2: Apparent viscosity as a function of CO_2 molar fraction for different qualities using AOS surfactant [1].

In order to better understand the reason for these observations, the surfactant type in this study was altered to a non-ionic type. This was done to determine whether these observations were caused by the nature of the surfactant used.

2.2 Thesis outline

Chapter 3 outlines the procedures followed for each study in this thesis.

Chapter 4 is a summary of the results obtained from the quality scan experiments by changing the surfactant type to a non-ionic type. This chapter shows how the quality scans are affected by changing the nature of the surfactant at different CO_2-decane molar compositions.

Chapter 5 deals with foam generation in a surfactant filled core at different CO_2-decane molar compositions for a constant quality (50%). It shows that the pore volume of total injection that triggers a rise in pressure gradient is independent of the CO_2-decane molar compositions in the presence of decane at a quality of 50%. Further investigation shows that for a CO_2-decane composition of 80%, the volume of CO_2-decane mixture required to trigger a rise in pressure gradient is independent of the foam quality.

Chapter 6 deals with the effect of flow rate on foam at four different CO_2-decane mixture compositions, at 50% quality. All tested CO_2-decane mixture compositions are found to be shear thinning. The effect of flow rate on a complete quality scan at a CO_2 -decane composition of 80% is also studied. It shows that the apparent viscosity decreases with increase in Darcy velocity along the entire range of qualities.

Chapter 7 shows the effect of permeability on supercritical CO_2 foam in the presence and absence of decane. It shows that for a reduced permeability and at a constant flow rate and quality, the CO_2 and CO_2-decane mixture pore volumes required to trigger a rise in pressure drop during foam generation decreases. The injected pore volume required to trigger the rise in pressure drop was therefore, among other things, dependent on flow path dimensions. This chapter also explores possible formation damage due to the formation of carbonic acid.

Chapter 8 summarises the main conclusions from each study in the thesis.

Chapter 9 outlines the practical implications of the results in the thesis.

Chapter 10 is a summary of the recommendations made for further investigation as a result of the observations made in this thesis.

3 Experiments

3.1 Materials and Apparatus

The non-ionic surfactant used was Alkyl Polyglucoside (APG) (Triton® CG-650 surfactant) with 50% active matter. The surfactant was used at a concentration of 0.5 wt. %, which is well above the CMC of 0.01% at 19°C, and brine composition of 1 wt.% Sodium chloride (shown in Appendix E). The oil used was decane (EMD Millipore Corporation, CAS-No: 124-18-5) with a density and viscosity of 722.38 kg/m^3 and 0.766 cP at 40°C respectively. The gas used to conduct the experiments was 99.7 vol % pure CO_2. Bentheimer and Berea sandstones were used as porous media. Figure 3.1 shows a schematic of the core. The total length of the core was 17 cm, with a radius of 3.8 cm and 3.7 cm for the Bentheimer and Berea cores respectively. The permeability of the cores were calculated using the Darcy equation (as shown in Appendix B)

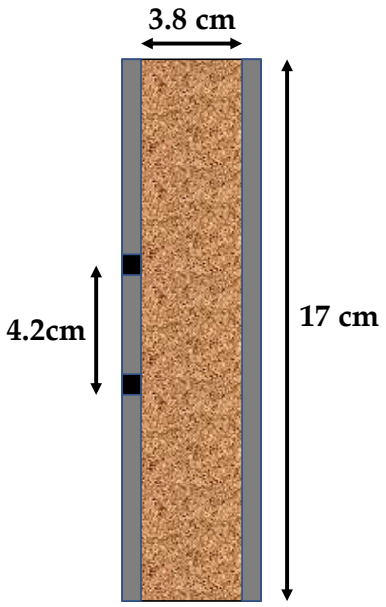

Figure 3.1: Schematic of the core

Figure 3.2 is a schematic of the experimental apparatus used in this study.

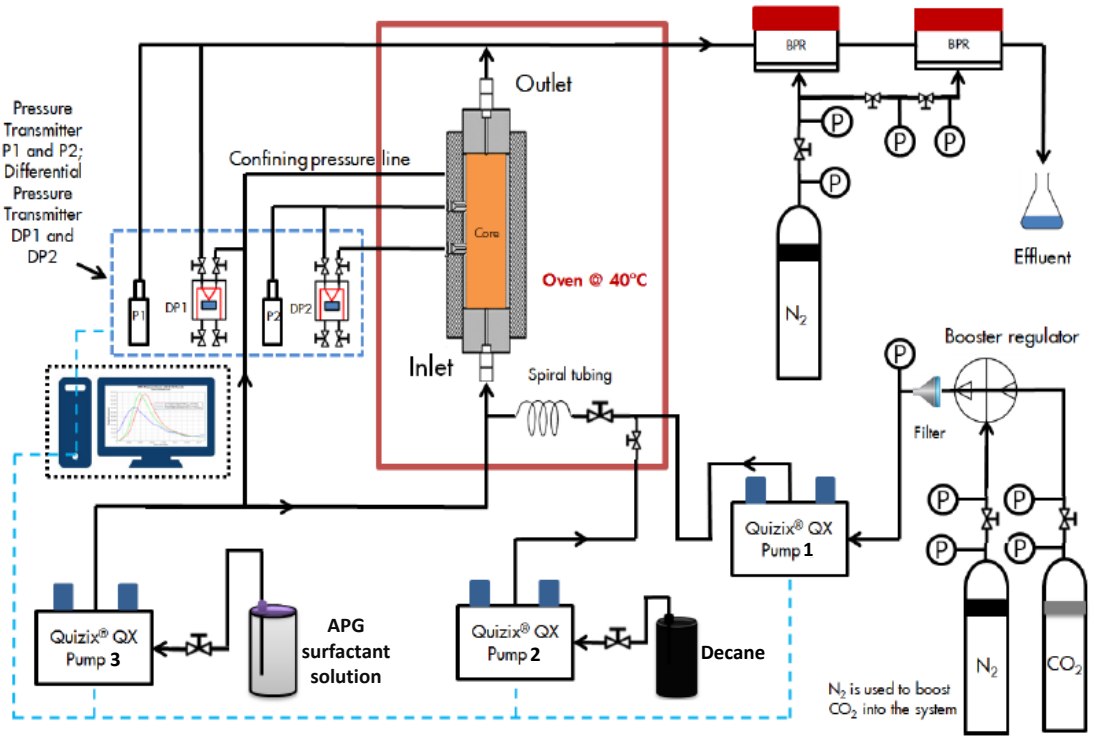

Figure 3.2: Schematic of experimental apparatus

The Bentheimer/Berea sandstone core is held in a cylindrical core holder. The core is coated in glue to seal it. Pressure transducers are connected to the core through holes drilled through the glue. The core holder is placed in an oven and set up such that the flow is from the bottom to the top. Decane and APG surfactant are injected into the core at constant rates using Quizix™ QX-6000 pumps 2 and 3 respectively. A booster regulator provides CO_2 through pump 1. The spiral tubing provides sufficient mixing of CO_2 and decane before entering the core. To control the pressure changes due to the phase change of CO_2 from liquid to gas, two back pressure regulators are used. The pressure and flow rate data was collected and recorded. The experiments were carried out at 90 bar and 40^0C.

3.2 Experimental Procedure

For this study, 3 types of experiments were conducted as outlined below;

3.2.1 Quality scan experiments

At least 10 PV of the APG surfactant solution was first injected in Bentheimer cores to fulfil rock adsorption. CO_2-decane mixtures of different molar compositions (XCO_2 = 100%, 95%, 80%, 50%, 20% and 0%) were made to mimic oil and gas interaction in a reservoir. The mixture was then co-injected with surfactant solution at a total flow rate of 1ml/min. The experiments were randomly ordered at different CO_2 -decane mixture fractional flows or foam quality. In these experiments, quality (*f*) refers to the ratio of gas, oil or gas-oil mixture volumetric flow rate to the total volumetric flow rate. The qualities were determined as follows;

$$f_{mix} = f_{gas} = \frac{q_{gas}}{q_{gas} + q_w} \quad \text{at } XCO_2 = 1 \tag{3.1}$$

$$f_{mix} = \frac{q_{mix}}{q_{mix} + q_w} \quad \text{at } 0 < XCO_2 < 1 \tag{3.2}$$

$$f_{mix} = f_{oil} = \frac{q_{oil}}{q_{oil} + q_w} \quad \text{at } XCO_2 = 0 \tag{3.3}$$

Where q_{gas}, q_{oil}, q_w, q_{mix} are the volumetric flow rates of CO_2, decane, APG surfactant solution and CO_2-decane mixture respectively. Note that f_{mix} was termed f_{gas} in experiments where CO_2 alone was co-injected with surfactant solution and f_{oil} in experiments where decane alone was co-injected with surfactant solution. The CO_2 flow rate was corrected for brine solubility based on the pressure and temperature (as shown in Appendix D). The term 'mixture experiments' will be used to refer to experiments where a CO_2-decane mixture was co-injected with surfactant solution.

The foam mobility reduction capabilities were quantified through an apparent viscosity value using Darcy's equation;

$$\mu_{app} = \frac{k.A.\Delta p}{q_{total}.L} = \frac{k.\nabla P}{u_{total}} \tag{3.4}$$

Where ∇P is the pressure gradient, k is the permeability and u_{total} is the total velocity. Unless otherwise indicated, the pressure drop along the mid-section of the core (4.2 cm) was used for the calculation of apparent viscosity. A new core was used for each CO_2-decane molar composition.

3.2.2 Foam generation experiments

Foam generation experiments were conducted in Bentheimer cores for CO_2-decane molar compositions of XCO_2= 100%, 95%, 80% and 20%. The point at which foam generation was initiated as well as its propagation along the core were studied to understand the behaviour of the dispersed phase.

Before each foam generation experiment, a new core was pre-flushed with 10 PV of surfactant solution to fulfil adsorption. CO_2 or CO_2-decane mixture was co-injected with surfactant solution into the core at a total flow rate of 0.1ml/min and a gas/mixture quality of 50%. The rise in pressure gradient for the 4 different CO_2-decane molar compositions was then observed.

Furthermore, the foam generation experiment for the CO_2-decane mixture composition of XCO_2= 80% was repeated at a quality of 10% and compared to the foam generation experiment at a quality of 50%.

3.2.3 Flow rate experiments

After steady state was reached in the foam generation studies, the flow rate was increased from 0.1 ml/min to 0.2, 0.4, 0.6, 0.8 and 1 ml/min, for the 4 tested CO_2-decane molar compositions. The corresponding apparent viscosity values were calculated at each flow rate.

To study the shear-thinning behaviour along the XCO_2=80% quality scan, 3 complete quality scans were carried out consecutively, with increasing flow rate. from 0.7, 1.6 and finally 2.4 ml/min.

A core was first pre-flushed with at least 10 PV of surfactant solution to satisfy adsorption. A CO_2-decane mixture then was co-injected with surfactant solution into the core. A complete quality scan was made each time before moving on to a higher flow rate. The pressure drop at steady state was used to calculate the apparent viscosity at each quality.

3.2.4 Permeability experiments

An attempt at generating supercritical CO_2 foam was made in Berea sandstone cores of 202mD and 184mD permeability. The cores were first pre-flushed with 10 PV of surfactant solution to fulfil adsorption. CO_2 (experiment A) and CO_2-decane mixture at XCO_2=80% (experiment B) were co-injected with surfactant at a quality of 50% and total flow rate of 0.1 ml/min in the 2 cores respectively. The flow rate was later increased to 0.2 and 0.4 ml/min in experiment A, before the experiment was terminated.

4 Effect of surfactant type

4.1 Results and discussion

Figure 4.1 is a summary of the apparent viscosity as a function of quality using APG surfactant solution at different CO_2-decane molar compositions. All tested CO_2-decane molar compositions show that the apparent viscosity gradually increases with foam quality in the low-quality regime and decreases with foam quality in the high-quality regime.

There is a sharp increase in apparent viscosity as the quality approaches transition quality (0.95) in the XCO_2=100% quality scan which is absent in the experiments with AOS surfactant. The apparent viscosity increases from 250cP to 400 cP for an increase in quality from 0.9 to 0.95.

In addition, the transition foam quality with APG surfactant (0.95) is higher than that with the AOS surfactant (0.9). The foam formed by APG was therefore more stable at high gas fractional flow rate than foam formed with AOS surfactant. The difference in the permeability and flow rate between the experiments with APG and AOS surfactants cannot be ruled out as having affected the difference in transition foam quality. The effect caused by the difference in permeability is such that high permeability is synonymous with a higher foam apparent viscosity although this effect is greatly reduced or absent at high permeability values [71, 72].

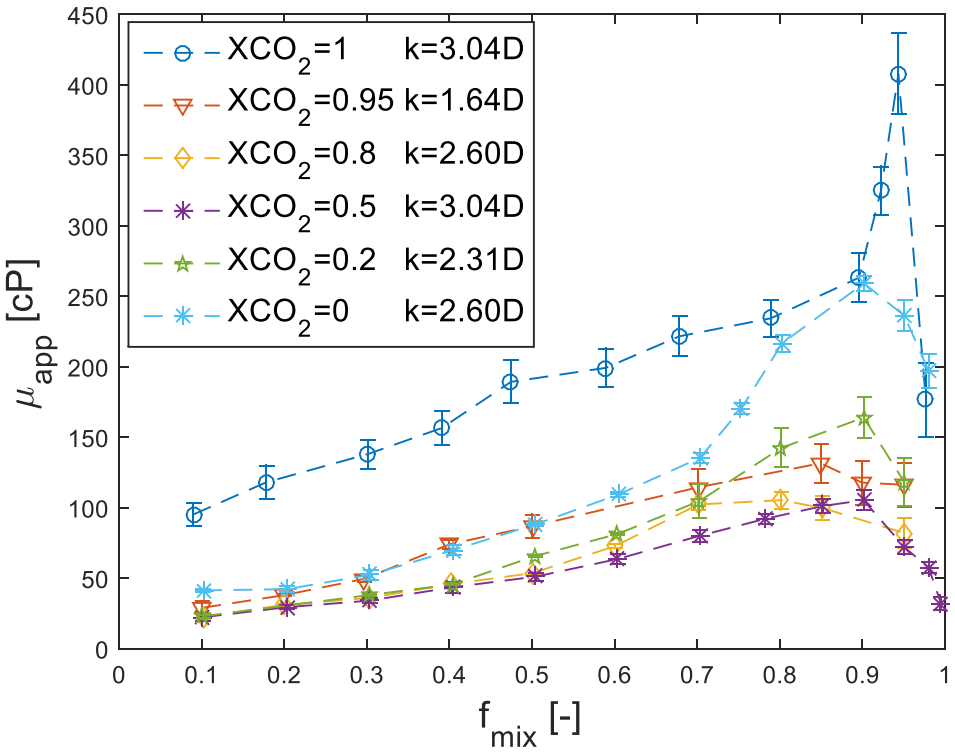

Figure 4.1: Apparent viscosity as a function of quality at different CO_2-decane molar compositions using APG surfactant.

The quality scans using APG and AOS surfactant solution at $XCO_2 = 0\%$ agree with a study by Uzoigwe and Marsden [70] which showed that the apparent viscosity of emulsions increases with quality in the low-quality regime. Both experiments with APG and AOS surfactants showed the presence of a high-quality regime.

The results in this study show the presence of both the high and low-quality regimes for the range of CO_2 molar fraction between 20% and 80% which is not the case with AOS surfactant. The experiments using AOS surfactant showed that this region exhibited only a low-quality regime.

When the apparent viscosity is plotted as a function of the CO_2 molar fraction in the CO_2-decane mixture (shown in Figure 4.2), three different regions are observed as in experiments with AOS surfactant. For $XCO_2 < 20\%$, the apparent viscosity decreases with increase in the CO_2 molar fraction while for $XCO_2 > 80\%$, the apparent viscosity increases with increase in CO_2 molar fraction. For $20\% < XCO_2 < 80\%$, the apparent viscosity seemingly remains unchanged with varying CO_2 molar fraction. Unlike in experiments with AOS surfactant, there is an increase in apparent viscosity with increase in quality in the low-quality regime in all tested CO_2-decane molar compositions with APG surfactant.

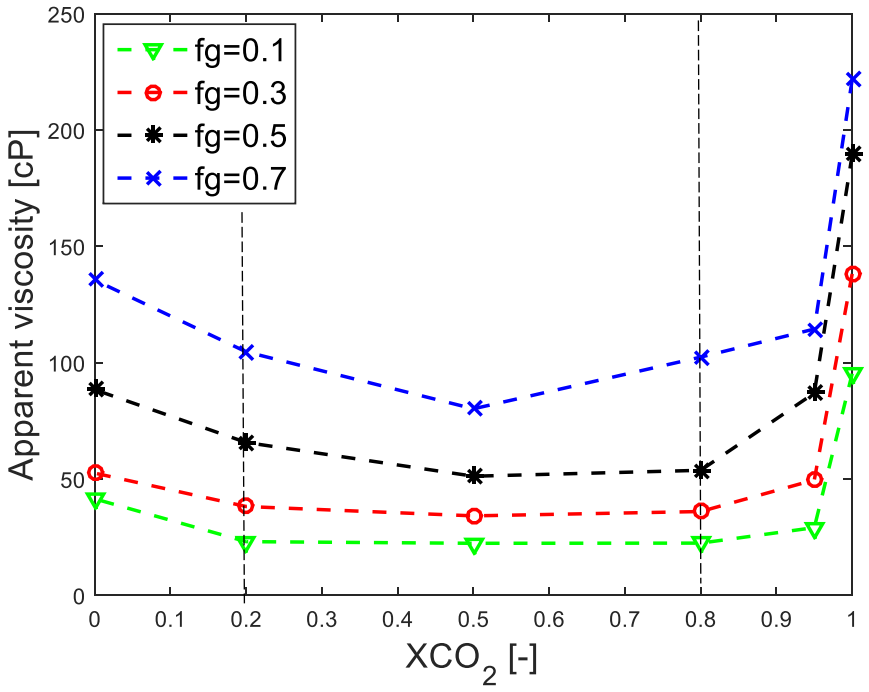

Figure 4.2: Apparent viscosity as a function of CO_2 molar fraction at different qualities.

It is important to note that for cases involving the injection of decane, the experiments produced significant amounts of emulsions in the effluent. It is therefore difficult to determine the contributions (in magnitude) to the measured pressure drop made by foam and by emulsions through a core flooding experiment.

Figure 4.3 shows a comparison between quality scans for the two surfactant types at $XCO_2 = 80\%$ at a total flow rate of 1.6ml/min. The increase in apparent viscosity of foam/emulsion with increase in quality in the low-quality regime can be observed in the APG surfactant experiment. There is also a high-quality regime where the apparent viscosity drops with increase in quality, a trend that is absent in the

experiments with AOS surfactant. This behaviour could likely be due to 'phase inversion', a term that will be described later on.

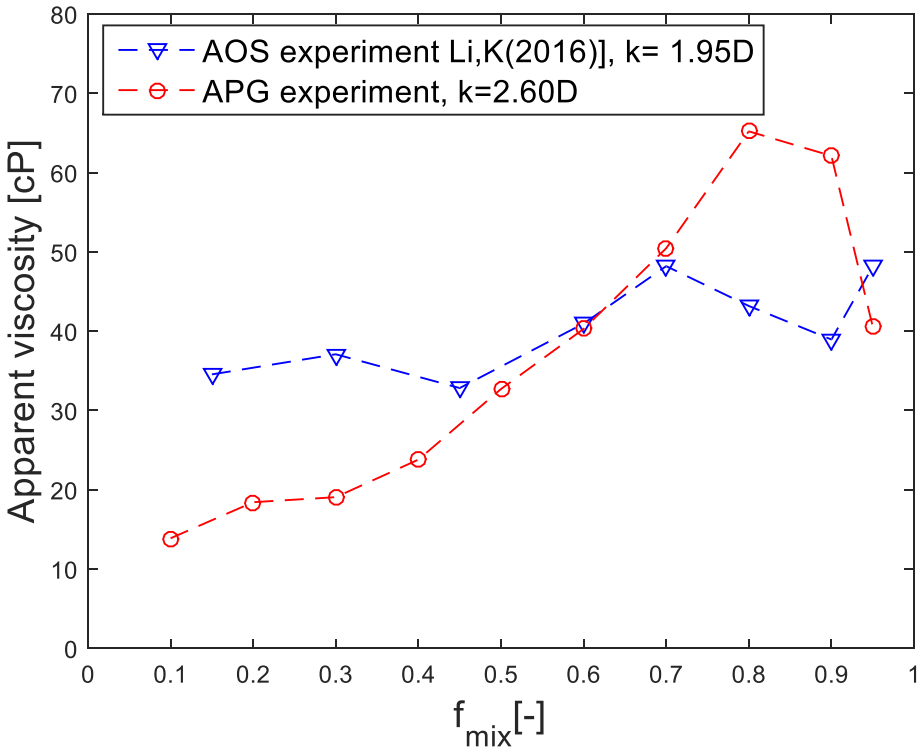

Figure 4.3: Apparent viscosity as a function of quality for AOS and APG surfactants at XCO_2 =80%

Figure 4.4 is a comparison between quality scans using APG surfactant for and XCO_2=80% at a constant total flow rate of 1ml/min. It shows that emulsions formed when decane alone is co-injected with surfactant solution create a higher apparent viscosity compared to experiments where CO_2 is present. Both quality scans with and without CO_2 exhibit the low and high-quality regimes.

The apparent viscosity of foam increases with quality due to increased bubble trapping in the low-quality regime while in the high-quality regime, the limiting capillary pressure is reached causing rapid bubble coalescence and a reduction in apparent viscosity [1].

Generally, the viscosity of an emulsion (XCO_2=0%) increases with increase in the dispersed phase fraction/concentration [73]. The sudden decrease in apparent viscosity is likely because of emulsion 'phase inversion'. Phase inversion is initiated by changing factors such as the temperature or electrolyte concentration of an emulsion system, or as in this case, increasing the volume fraction of the dispersed phase [74]. Catastrophic phase inversion occurs at a critical dispersed phase volume fraction, $\emptyset_{Cr}$, also known as the maximum packing fraction. Beyond $\emptyset_{Cr}$, the oil-in-water emulsion viscosity decreases because the emulsion suddenly has a much lower volume fraction of dispersed phase (water-in-oil) [74]. Tadros shows that the continuous phase is oil by measuring the conductivity of the emulsion in the high-quality region. The measured conductivity is low because the continuous phase, oil, is less conductive than water.

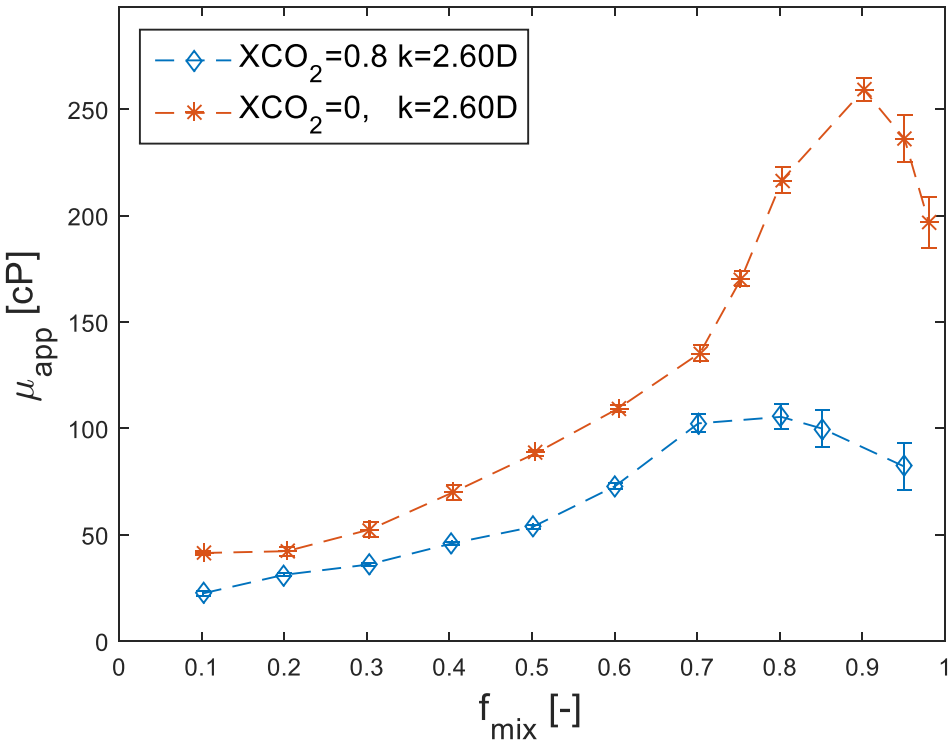

Figure 4.4: Apparent viscosity as a function of quality for XCO_2=0.8 and XCO_2=0 at 1ml/min.

5 Foam generation

Transient foam generation experiments were carried out to study how foam is generated under miscible conditions.

5.1 Results and Discussion

Figure 5.1 shows the pressure gradient as a function of the total pore volumes of injection for four tested CO_2-decane molar compositions.

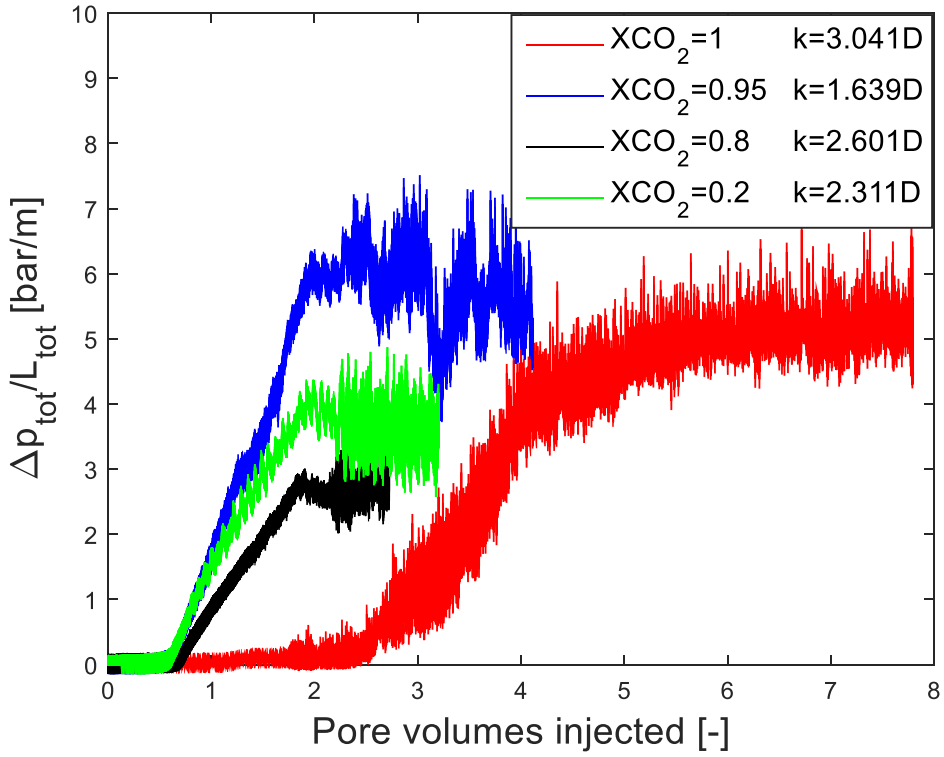

Figure 5.1: Pressure gradient as a function of PV injected for different CO_2 molar compositions

In the CO_2-decane mixture experiments, the pressure gradient appeared to suddenly increase at 0.6 PV to 1.7 PV of total injection, independent of the CO_2 molar fraction in the mixture (shown in Figure 5.1). All three tested CO_2-decane mixture compositions generally showed a linear increase in pressure gradient and finally reached steady state after about 1 PV from the point at which the rise began. This suggests that the foam/emulsion is created with a stable front as it advances to the outlet. As a result, the pressure gradient takes roughly about 1 PV to reach steady state.

A closer look at the foam/emulsion generation point in Figure 5.2 shows that the pressure gradient is in fact increasing from time 0 PV, but at a very slow rate. This could indicate that weak foam may be initially formed.

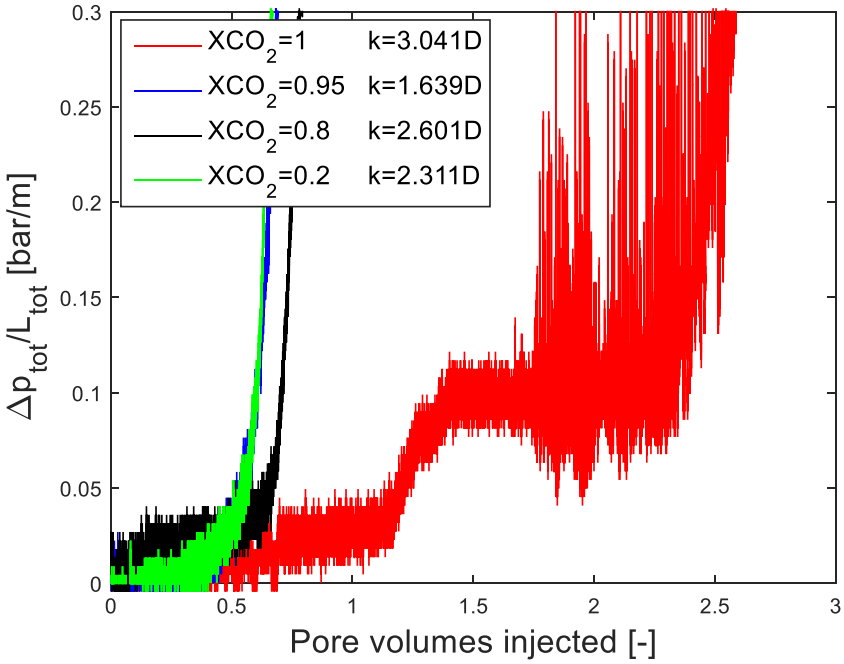

Figure 5.2: Pressure drop vs PV injected for the first 3 Pore volumes

For pure CO_2 injection (shown in red in Figure 5.2), the pressure gradient rises to 0.1 bar/m after about 1.5 PV of total injection and remains steady for 1 pore volume. This could indicate that weak foam is first formed throughout the core followed by rapid formation of strong foam at 2.5PV. This delay in the rise of the pressure gradient prior to the injection of 1.5 PV may be due to several reasons as explained below.

Some of the injected supercritical CO_2 may dissolve in the surfactant solution in the pore space which may affect foam generation. 1PV of surfactant solution would ideally dissolve 0.11 PV of CO_2 at the prevailing experimental conditions (see Appendix D). It is believed that the dissolution of CO_2 decreases the solubility of surfactant in water which alters the interfacial tension hence decreasing the pressure drop caused by generated foam [75].

Another reason for the delay in formation of strong foam could be because CO_2 is highly diffusive [76]. This allows it to easily move across liquid films resulting in coarsening and formation of weak foam. With continued injection, the weak foam may then transition to stronger foam at 2.5 PV of injection. This occurs at a pressure gradient of 0.1 bar/m.

The CO_2-decane experiments show that the total injected pore volume required before a rise in pressure gradient (approximately 0.6 PV) is observed is independent of the CO_2-decane molar composition (shown in Figure 5.2). Results from the foam generation experiments of the CO_2-decane molar composition XCO_2=80%, are presented at two different qualities i.e. 10% (k=2.99D) and 50% (k=2.60D) (shown in Figure 5.3). When the pressure gradient was plotted against the injected CO_2-decane mixture pore volume, the results showed that the pressure gradient increased sharply at the same injected CO_2-decane mixture volume, 0.3 PV, regardless of the quality.

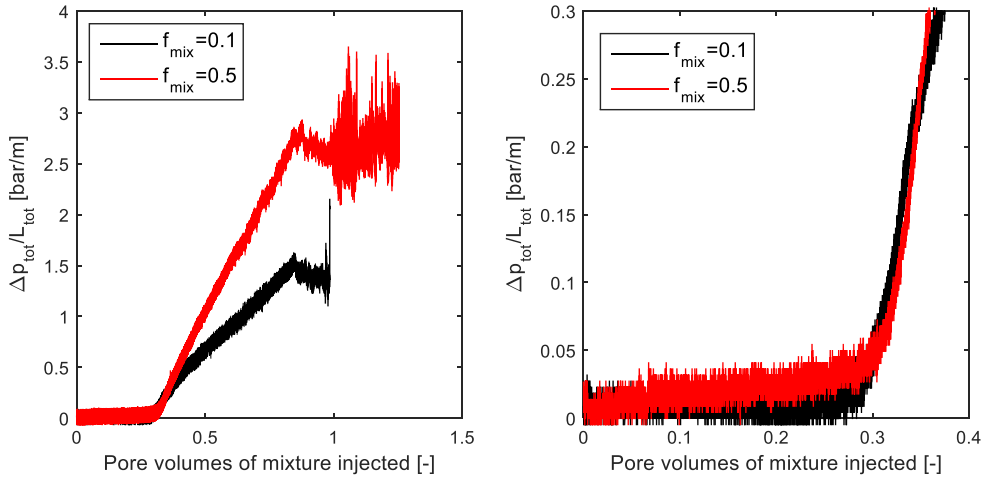

Figure 5.3: Pressure gradient as a function of mixture pore volume injected for XCO_2 =80% at time 0-1.5PV [left] and time 0-0.4PV [right]

A closer look at the 'trigger point' which occurs when about 0.3 PV of the CO_2-decane mixture has been injected into the core is shown on the right in Figure 5.3 . The absence of a significant pressure gradient prior to this volume of mixture injected may be attributed to the 'entrance effect' as earlier stated. The entrance effect is defined by Nguyen [77] as a poor foam development phenomenon near the inlet region of a core during foam generation. When gas is injected into a surfactant-filled core, the gas enters the largest pores first due to the low capillary entry pressure in the larger pores compared to small ones. These large pores in turn shape the gas into a coarse texture due to their large size which creates weak foam. The gas then flows into smaller pores due to the increase in the pressure gradient. This invasion of gas into the pores in the inlet section allows liquid saturation to fall gradually and is controlled by the rate of foam generation [77].

6 The effect of flow rate

Foams and emulsions in porous media are generally shear-thinning in nature [10, 31, 64, 68] but little is known about how oil affects this behaviour under miscible conditions. To this end, experiments using APG surfactant were carried out to study the effect of flow rate at a constant quality (50%) for different CO_2-decane molar compositions (XCO_2=100%,95%,80% and 20%) as well as the effect of flow rate on the shape/behaviour of the XCO_2=80% quality scan.

6.1 Results and discussion

For all tested CO_2-decane molar compositions (shown in Figure 6.1), the 50% quality was found to be shear-thinning in nature with a similar slope when the flow rate was increased. The increase in flow rate increases the pressure gradient that mobilises trapped bubbles which in turn lowers the apparent viscosity.

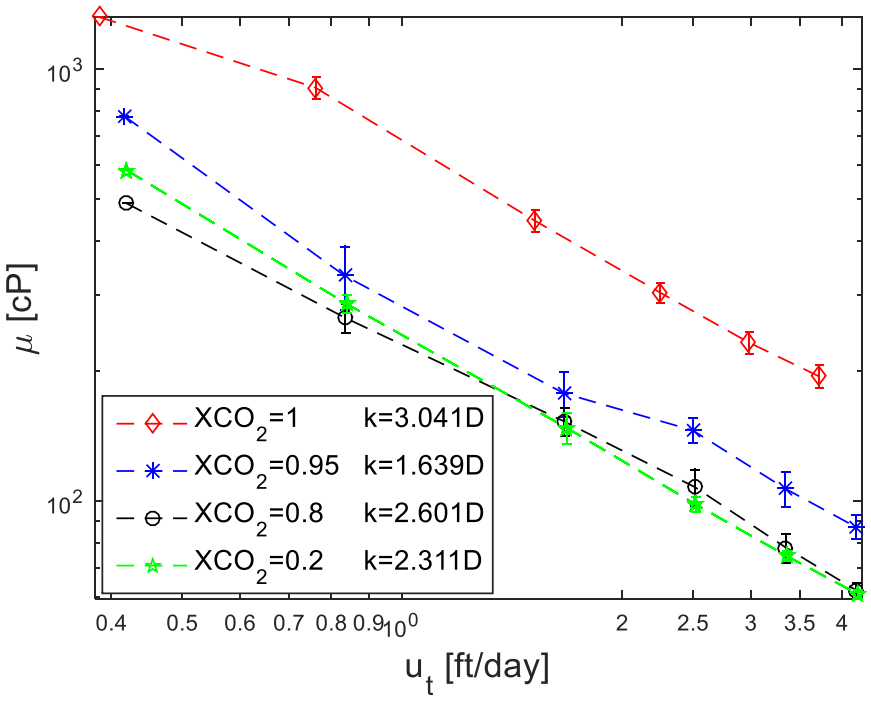

Figure 6.1: Apparent viscosity as a function of superficial velocity at 50% quality.

The results showed that the variation of apparent viscosity with superficial velocity can be independent of the CO_2-decane mixture composition for the prevailing experimental conditions. The CO_2-decane molar compositions of 80%, 95% and 20% have comparable apparent viscosities which suggests that the foams may not differ in interfacial tension properties. This could be as a result of using the surfactant solution at a concentration high above CMC which might create a kind of 'interfacial tension buffer' enabling the foam/emulsion formed to have similar flow properties regardless of the difference in CO_2 molar fraction in the mixture.

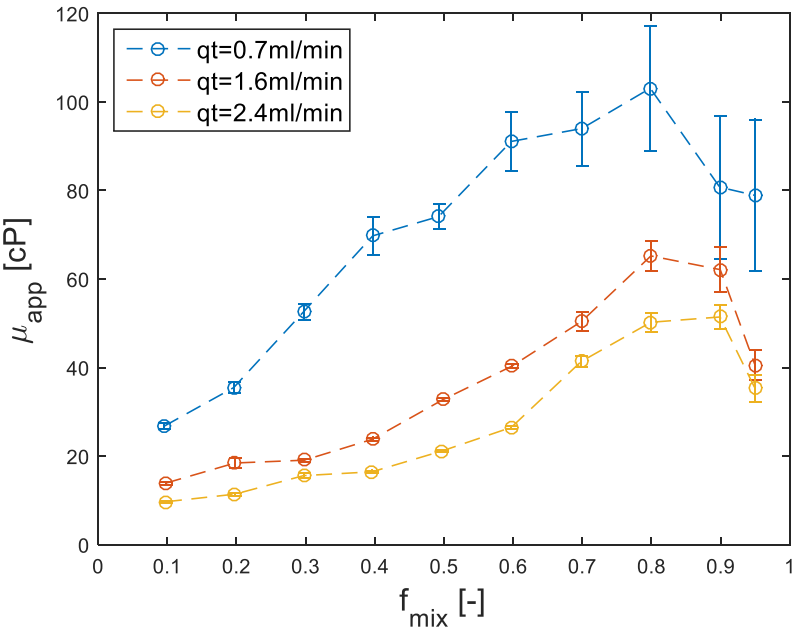

Figure 6.2: Quality scans at increasing flow rates for XCO_2 =0.8

The results (shown in Figure 6.2) showed that the apparent viscosity increased with quality to a maximum and then decreased with quality. The increase was more pronounced at low shear rate as observed in literature [70]. The results revealed the presence of a high-quality regime, contrary to the findings of Kahrobaei et al. [1]. where it was absent.

In addition, all qualities were shear-thinning in nature. The apparent viscosity of each quality decreased when the total injection rate was increased. The results showed that both the low and high-quality regimes remain present as the total flow rate increased. This behaviour was determined to be a result of the surfactant type.

A closer look at the pressure drop for the three quality scans (shown in Figure 6.3), shows that for qualities $\leq$ 60%, the flow exhibits more shear-thinning behaviour compared to qualities above 60%. This shear-thinning tendency can be modelled using the power law.

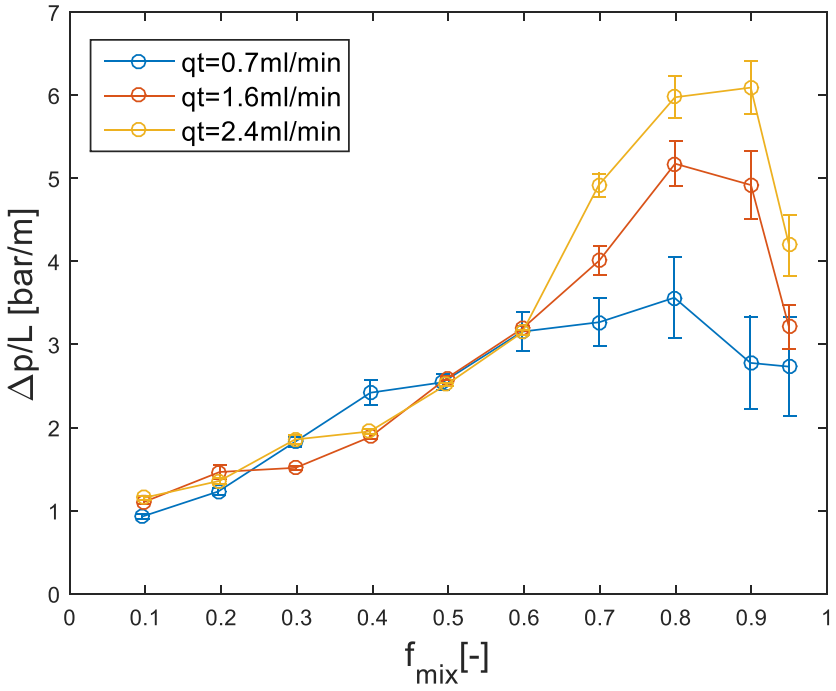

Figure 6.3: Pressure gradient as a function of quality at increasing flow rates (XCO_2=80%)

6.1.1 Determination of Coefficients of power-law fluid model

The power law fluid model was used to express the relationship between the apparent viscosity and shear rate for the experiments above.

The power law model relates the apparent viscosity to shear rate as follows [78, 79];

$$\mu_{app} = K\gamma^{n-1} \tag{6.1}$$

Where μ_{app} is the apparent viscosity, K is the consistency factor, γ is the shear rate and n is the flow behaviour index. Values of n range between 0 and 1, with the more shear thinning fluids having values of n closer to 0. Shear rate can be related to Darcy velocity through the following relation;

$$\gamma = \left(\frac{1+3n}{n}\right)\frac{u_{total}}{\sqrt{8k\varphi}} \tag{6.2}$$

Where u_{total} is total Darcy velocity, k is rock permeability and φ is porosity. The apparent viscosity in porous media is therefore calculated as;

$$\mu_{app} = K\left(\left(\frac{1+3n}{n}\right)\frac{u_t}{\sqrt{8k\varphi}}\right)^{n-1} \quad (6.3)$$

By the method of least square error, the values of n and K were obtained. Figure 6.4 shows a fit of experimental data to calculated values of Apparent viscosity based on obtained values for n and K for a quality of 0.2 and CO_2 molar fraction of 80%.

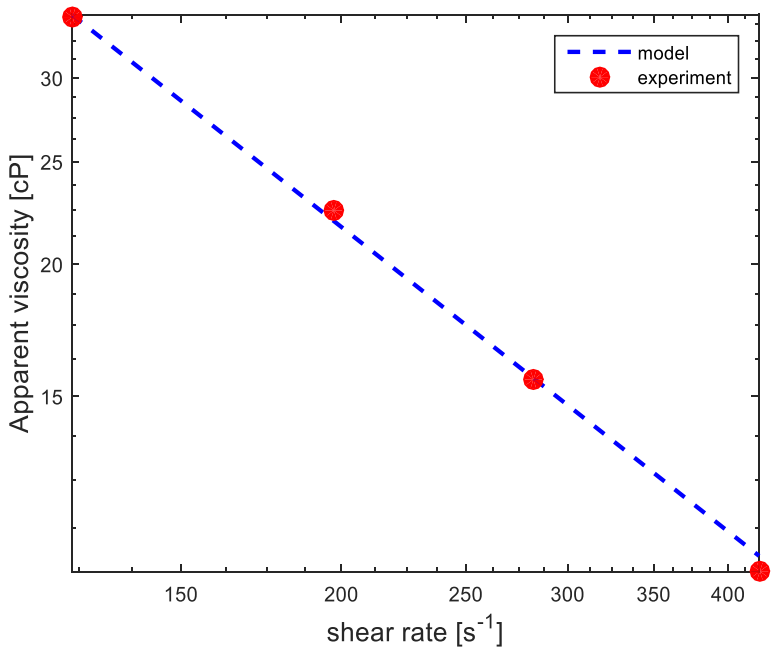

Figure 6.4: Apparent viscosity versus shear rate for the experimental data and model parameter fitting (n= 0.0435 and K= 691.8046)

n and K values for all qualities were determined similarly and are tabulated in Table 6.1.

Table 6.1: Values of n and K for XCO_2=80% at each quality

f_{mix}	n	K
0.1	0.1308	425.6823
0.2	0.0435	691.8046
0.3	1.8610e-09	6.2143e+10
0.4	3.8382e-09	2.3106e+11
0.5	0.0643	1.0408e+04
0.6	0.1465	5.5912e+03
0.7	0.3852	864.5158
0.8	0.4483	644.9982
0.9	0.6365	232.4671
0.95	0.3670	754.6299

Chapter 6. The effect of flow rate

Generally, the shear-thinning tendency appears to reduce above the 60% quality. The values of n for qualities $\leq$60% are found to range between 0 and 0.15, Above the 60% quality, the value of n increases with quality with a maximum at around transition quality and then drops with increase in quality in the high-quality regime.

7 The effect of permeability.

In this chapter, the effect of permeability on foam generation is studied. Berea sandstone was chosen due to its low permeability, in order to compare it to the foam generation results observed in the higher permeability Bentheimer sandstone in Chapter 5.

Previous experiments on the effect of permeability on foam have been successful with several authors [80, 71, 81] reporting a correlation between foam apparent viscosity and core permeability. Lee et al. [71] found that the apparent viscosity of CO_2 foam decreased with decrease in permeability. This relationship was found to be nonlinear and approached asymptotes at both high and low rock permeabilities. This observation is supported by the results obtained in works by Parlar et al. [72] who showed that the apparent viscosity of foam approaches a plateau at high permeabilities.

However, the work of Siddiqui et al. [81] showed that while foam can be generated in porous media of as low as 9 mD, there is a high risk of permanently damaging the formation. There was evidence of core property alteration and damage when CO_2 foam experiments were carried out using Berea sandstone. This was attributed to the formation of carbonic acid when supercritical CO_2 dissolves in surfactant solution.

The dissolution of injected CO_2 in water results in low water pH and dissolves minerals and organic matter. This is likely to cause damage to the formation or change the mechanical properties of the rock [82, 83]. Iglauer et al. [84] observed an increase in pressure drop when Berea cores were flooded with CO_2-saturated brine and an even higher increase with supercritical CO_2. Fines release, migration and pore blocking were cited as the main causes of the observed permeability reduction of up to 35%. Moreover, higher permeability reduction was observed at higher flow rates. Core flooding experiments by Mohammed et al. [85] showed that CO_2 injection led to a 55% decrease in permeability in Berea cores. Filtration of the effluent showed precipitated materials like calcium and iron. This was attributed to the action of carbonic acid on clays and cements. Experiments involving the application of CO_2 foam in both fired and unfired Berea and unfired Boise sandstone have observed a reddish colour as well as small particles in the effluent [86]. This was attributed to the dissolution of minerals (iron) due to the formation of carbonic acid.

7.1 Results and Discussion

Figure 7.1 shows the pressure gradient along the total length of the core as a function of total pore volumes injected for XCO_2=100% (experiment A) at a rate of 0.1ml/min.

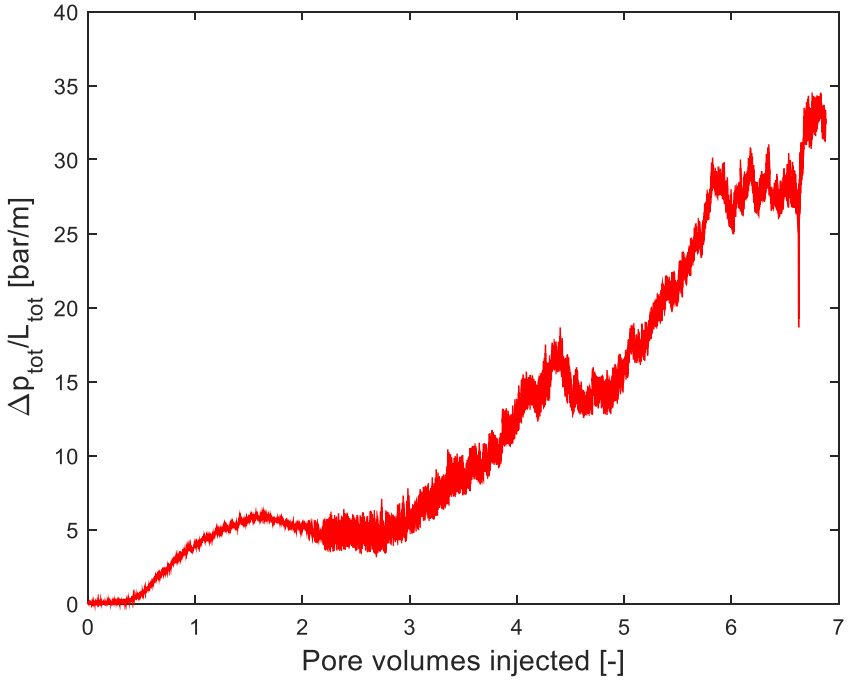

Figure 7.1: Pressure gradient as a function of total pore volumes injected at 50% quality

Initially, the pressure gradient rose after about 0.4PV of total injection to approximately 5 bar/m and held for 1.5PV; after which it suddenly rose to 17bar/m and later 30bar/m after 6PV of injection. The pressure gradient then remained steady for about 1 pore volume corresponding to an apparent viscosity of 412 cP. In comparison, the same experiment in Bentheimer sandstone reached steady state at about 1000 cP.

The ‘trigger’ total pore volume required to initiate a pressure drop was found to have reduced with a decrease in permeability i.e. 0.4 PV at 202 mD as opposed to 2.5PV at 3.04 Darcy.

Figure 7.2 shows the change in pressure gradient with increase in flow rate from 0.1 ml/min to 0.2 ml/min and finally 0.4ml/min, from left to right, separated by vertical red lines.

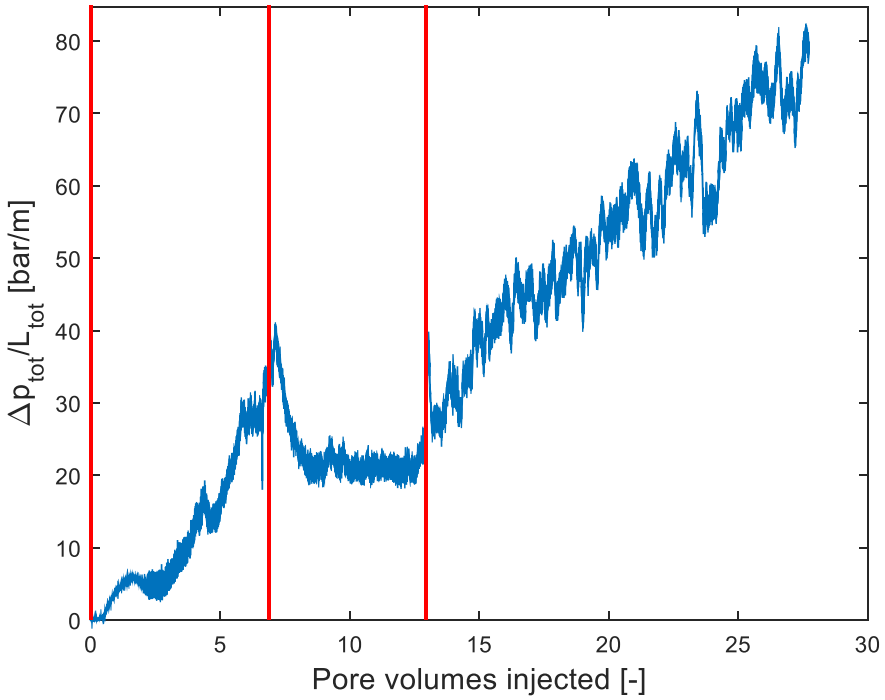

Figure 7.2: Pressure gradient as a function of total pore volumes injected at increasing flow rates (left to right: 0.1, 0.2, 0.4ml/min) separated by vertical red lines.

When the flow rate was increased from 0.1ml/min to 0.2 ml/min, the pressure gradient spiked to 40 bar/m and then dropped to about 23 bar/m corresponding to an apparent viscosity of approximately 151 cP. This flow rate presented with a less chaotic trend in pressure gradient compared to 0.1ml/min, remaining stable for at least 4 pore volumes. The flow rate was finally increased to 0.4 ml/min which caused a continuous increase in pressure gradient with no steady state. The experiment was terminated after 27 PV of total injection. At this point, the pressure drop had risen to almost 80 bar/m.

The initial core permeability was not recovered after flushing the system with brine. The final brine permeability of the core was 38mD. This could be an indicator of damage due to the action of carbonic acid on the rock grains and cement. The pressure gradient rose with increase in flow rate possibly caused by damage that occurs at increased flow rate as observed in previous studies [84].

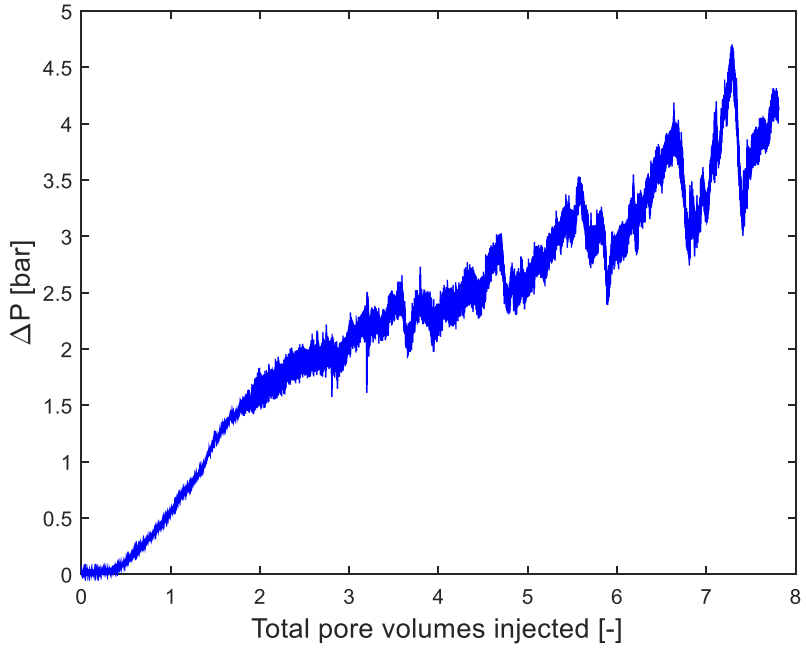

Figure 7.3: Pressure drop as a function of total pore volumes injected for XCO_2=80%, at a quality of 50% and total flow rate of 0.1 ml/min. (k=184mD)

Figure 7.3 shows the pressure drop over the total length of the core as a function of total pore volumes injected for the CO_2-decane mixture, XCO_2= 80%. The pressure drop begins to rise after 0.3PV of total injection, rapidly at first to 1.8 bar, and then slowly as injection proceeds. There is no observable steady state over the total section and the pressure drop increases as more CO_2-decane mixture and surfactant is injected.

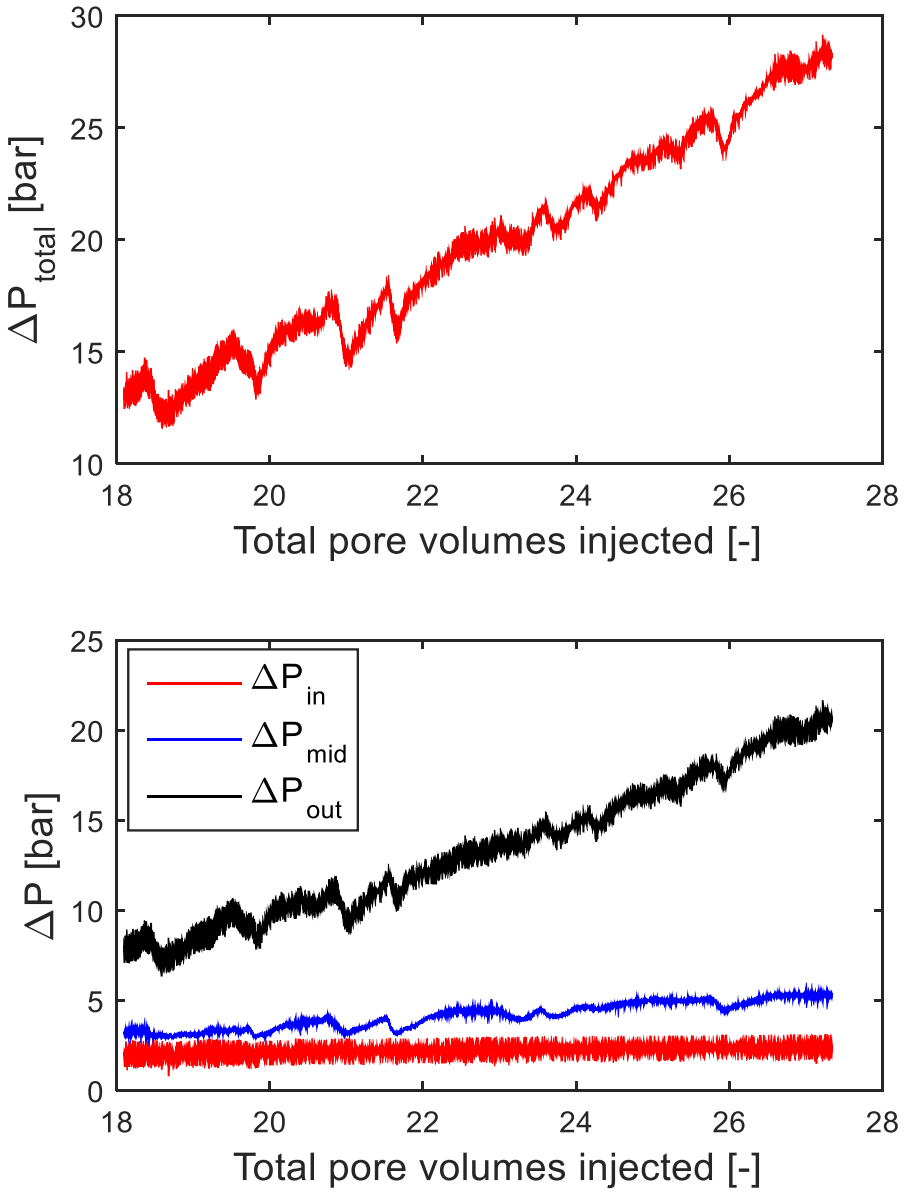

Figure 7.4: Pressure drop as function of Pore volumes for different sections

A closer look at the pressure drop in the different sections of the core (shown in Figure 7.4) reveals that with continued injection, the inlet and middle sections appear to reach a steady state. The pressure drop in the outlet section on the other hand continues to rise with injection. This behaviour shows that as the foam/emulsion proceeds to the outlet, it experiences an insufficient pressure gradient in the low permeability core as a result of radial flow. The foam/emulsion is therefore immobilised and it blocks the flow path.

At the same time, there is strong evidence of damage in the core. The observed pressure drop may not only be caused by foam/emulsions that plug the core but also fines release and migration and/or even swelling (see Appendix F). The permeability in experiment A drops from 202 mD before the experiment to 38 mD after the experiment while the pH of the surfactant solution changes from 10.76 before injection, to 4.97 in the effluent.

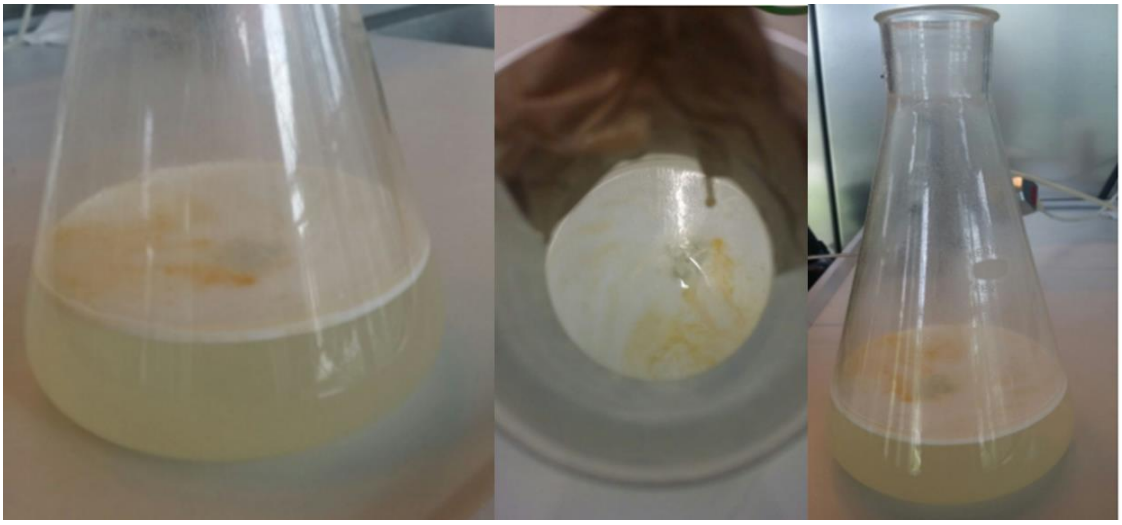

Figure 7.5: A brownish colour in the effluent because of the dissolution of heavy metals.

Figure 7.5 shows a brownish colour in the effluent from experiment B. This could be evidence of dissolution of heavy metals, most likely iron, due to the formation of carbonic acid when supercritical CO_2 dissolves in surfactant solution. A table showing the minerology of the Berea core is shown in Appendix F. The action of carbonic acid on the cement holding the grains together in Berea sandstones likely releases fines which cause damage to the formation by lodging in pore throats and increase the pressure drop required to mobilize the foam/emulsion. In addition, clay swelling cannot be completely ruled out as a contributor to the formation damage.

8 Conclusions

8.1 Effect of surfactant type

a) All quality scans with APG surfactant i.e. $0\% \leq XCO_2 \leq 100\%$ exhibit both the low and high-quality regimes. The CO_2-decane mixture quality scans i.e. $20\% \leq XCO_2 \leq 95\%$ using AOS surfactant lack the high-quality regime.

b) Quality scans for $XCO_2 = 100\%$ using APG show a change in behaviour near the transition quality. There is a rapid increase in foam apparent viscosity from 250 cP to 400cP for a change in quality from 0.9 to 0.95. This behaviour is absent in experiments using AOS surfactant.

c) The apparent viscosity in the CO_2-decane mixture scans i.e. $20\% \leq XCO_2 \leq 95\%$ is lower than in the pure CO_2 and pure decane quality scans. The flow resistance provided by CO_2 foam is therefore drastically reduced when the supercritical CO_2 is 'foamed' after it has been mixed with the oil.

d) The CO_2-decane mixture scans generally overlay each other showing that at the prevailing experimental conditions, the apparent viscosity in this regime is independent of the CO_2 molar fraction in the mixture.

e) Addition of supercritical CO_2 to decane (miscible conditions) in any proportion before foaming will create foams/emulsions that result into a lower apparent viscosity compared to emulsifying decane.

8.2 Generation studies

a) For the foam generation experiments with decane, the 50% mixture quality requires 0.6 PV of total injection to 'trigger' a rise in pressure gradient regardless of the CO_2 molar fraction in the mixture.

b) For the $XCO_2 = 80\%$ experiment, the 'trigger' mixture pore volume (0.3 PV) was found to be independent of quality.

c) Foam generation in the pure CO_2 experiment shows the presence of weak foam followed by rapid generation of strong foam.

d) Foam that is generated in the CO_2-decane mixture experiments appears to propagate across the core with a stable front. Steady state is reached within approximately 1 PV from the 'trigger' point.

8.3 Effect of flow rate

a) All tested CO_2-decane mixtures and pure CO_2 foam at 50% quality are shear-thinning. The apparent viscosity in the CO_2-decane mixture experiments decreases with the increase in superficial velocity and appears to be independent of the CO_2-molar fraction in the CO_2-decane mixture.

b) The increase in apparent viscosity with quality in the low-quality regime is more pronounced at low shear/flow rate.

c) All qualities are shear-thinning for the experiments using XCO_2=80%. The Power law model can be used to capture the effect of shear rate on the apparent viscosity of the foam/emulsions.

d) The shear-thinning tendency reduces considerably above the 60% quality.

e) Above the 60% quality, the shear-thinning tendency decreases with quality to a minimum around transition quality, and increases with quality in the high-quality regime.

8.4 Effect of permeability

a) A reduction in permeability led to earlier generation of foam/emulsions in the core. Less CO_2 and CO_2-decane mixture is required to initiate a rise in pressure drop in the Berea core compared to the Bentheimer core.

b) Berea cores are susceptible to blockage/plugging by foam away from the injection site caused by insufficient pressure gradients.

c) The blockage tendency in Berea cores increased with increase in flow rate as expected.

d) The original permeability was not recovered as expected probably due to core damage (from k=202mD to k=38mD) after supercritical CO_2 foam (XCO_2 = 1) was flushed out using brine.

e) A brown colour was observed in the effluent of the CO_2-decane experiment (B) which could be evidence of the effect of formation of carbonic acid on heavy metals (pH= 4.97).

9 Practical implications

a) CO_2-decane-surfactant floods with all tested CO_2 molar fractions can have an apparent viscosity above 25cP. This allows for a more stable displacement front in high permeability formations.

b) The shear-thinning tendency ensures good injectivity and better displacement away from the injection well as the apparent viscosity increases with decreased flow rate.

c) Generating foam in formations that have been pre-flushed with surfactant is affected by the permeability of the formation, with a lower permeability favoring faster formation of supercritical CO_2 foam.

d) Low permeability formations are susceptible to blockage/plugging by foams/emulsions at locations away from the injection site. Radial flow results in a reduced drawdown away from the well. Foams/emulsions that propagate deep into the formation therefore cannot be easily mobilized and will plug/block the flow path.

e) Foam/emulsion blockage could be accelerated by the presence of carbonic acid which promotes fines release and migration in formations containing clays. These fines may lodge in pore throats and increase the pressure gradient required to mobilize foam.

10 Recommendations

Based on the results of this study, recommendations are made as follows;

a) CO_2-decane quality scans have been found to have approximately the same apparent viscosity regardless of the CO_2 molar fraction in the mixture. It would be vital to understand whether this is still the case when the surfactant solution is used below CMC. Literature has shown that the interfacial tension of decane-water reduces linearly with the addition of supercritical CO_2 in the decane [13]. Using a surfactant at a concentration below CMC would provide insight into what would happen in the reservoir if surfactant is depleted for example through adsorption.

b) To obtain more reliable results for quality scans in low permeability cores, fired Boise sandstone or Fontaine blue sandstone cores may be used as they are less susceptible to the effect of carbonic acid [86].

c) Core flooding experiments in clay-containing cores such as Berea could be conducted with salts of different valency at different salinities to verify whether the effect of the clays can be mitigated in acidic conditions. Literature shows that the release of clay particles from Berea sandstone pore walls is strongly dependent on the type, concentration, and valency of the ions in the water injected [87].

Appendix

A. Leak test

a) The system is connected to a 7 bar helium line and the core is flushed with Helium gas for a few minutes.

b) The outlet valve is closed and snoop liquid is placed on the connections within the set up.

c) Leaks are identified by bubbling gas and the connections are carefully re-tightened.

d) The inlet valve is closed and the pressure in the system is monitored.

e) When there is no pressure drop to indicate gas leaks, the outlet valve is opened to release the helium.

f) The core is flushed with CO_2 gas for a few minutes and then vacuumed to -1.0 bar until the pressure in the core no longer changes.

g) The core is then saturated with 1wt% NaCl brine.

B. Permeability Measurement

a) After the core has been saturated with 1% NaCl brine solution, the system pressure is brought up to 90 bar and 40° C.

b) The permeability test is carried out by increasing the flow rates gradually through flow rate values of 0.5, 1, 2, 3, 4 and 5ml/min and then stepwise downward back to 0.5ml/min. Each flow rate is run for 10 minutes.

c) The permeability is calculated using Darcy's law;

$$k = \frac{Q\mu L}{A\Delta P} \qquad \text{(B.1)}$$

Where k is the permeability [D], Q is the flow rate cm^3/s], L is the length of the core [cm], A is the cross-section area off the core [cm^2], Δp is the pressure drop [atm].

The permeability of the cores for the quality scan experiments are summarised in Table B.1 below;

Table B.1: A summary of the permeability of the Bentheimer cores used for each CO_2-decane molar composition.

CO_2 molar fraction	**Bentheimer Core Permeability**
1	3.04D
0.95	1.63D
0.8	2.60D
0.5	3.40D
0.2	2.31D
0	2.60D

C. Experimental Procedure

a) Generation Studies (XCO_2= 100%, 95%, 80%, 20%)

- After the permeability test, the core is first pre-flushed with 10PV of surfactant solution to compensate for any adsorption.
- CO_2 or CO_2-decane mixture is co-injected with surfactant solution into the core at a constant CO_2-decane molar composition and quality.

b) Quality Scans (XCO_2= 100%, 95%, 80%, 50%, 20%, 0%)

- After the permeability test, the core is first pre-flushed with 10PV of surfactant solution to compensate for any adsorption.
- The quality scan is carried out at a constant total flow rate with varying qualities that are randomly ordered.
- Qualities are randomly chosen for repetition to ensure that the pressure drops are approximately as measured before.
- The core is replaced before experiments of a different CO_2-decane molar composition are carried out.

c) Flow rate experiments (XCO_2= 100%, 95%, 80%, 20%)

- The core is first pre-flushed with at least 10PV of surfactant solution to compensate for adsorption.
- CO_2 or CO_2-decane mixture is co-injected with surfactant solution at increasing flow rates from 0.1, 0.2, 0.4, 0.6, 0.8 to 1 ml/min.
- The pressure drop at steady state is recorded.

D. CO_2 solubility determination

The solubility of CO_2 in water was compensated in all surfactant flow rate calculations based on a study by Hangx (2005). The study compared a model by Duan and Sun [88] with past experimental data for CO_2 solubility in water and brine [89]. Figure D.1 shows that generally, CO_2 solubility in water increases with increase in pressure at constant temperature. In addition, the solubility decreases with increase in temperature below 100° C and increases with temperature above 100° C.

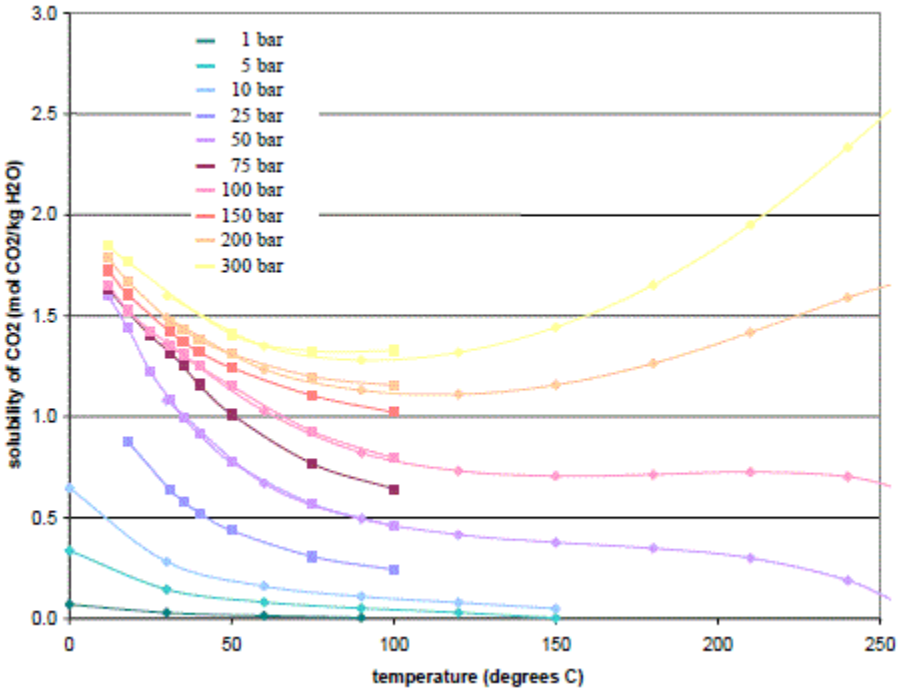

Figure D.1: CO_2 solubility as a function of Pressure and Temperature [89]

E. CMC determination

The CMC of the surfactant in 1wt% NaCl brine solution at 19°C was determined using a tensiometer. The surface tension of the solution was determined at different concentrations and plotted as shown in Figure E.2 below;

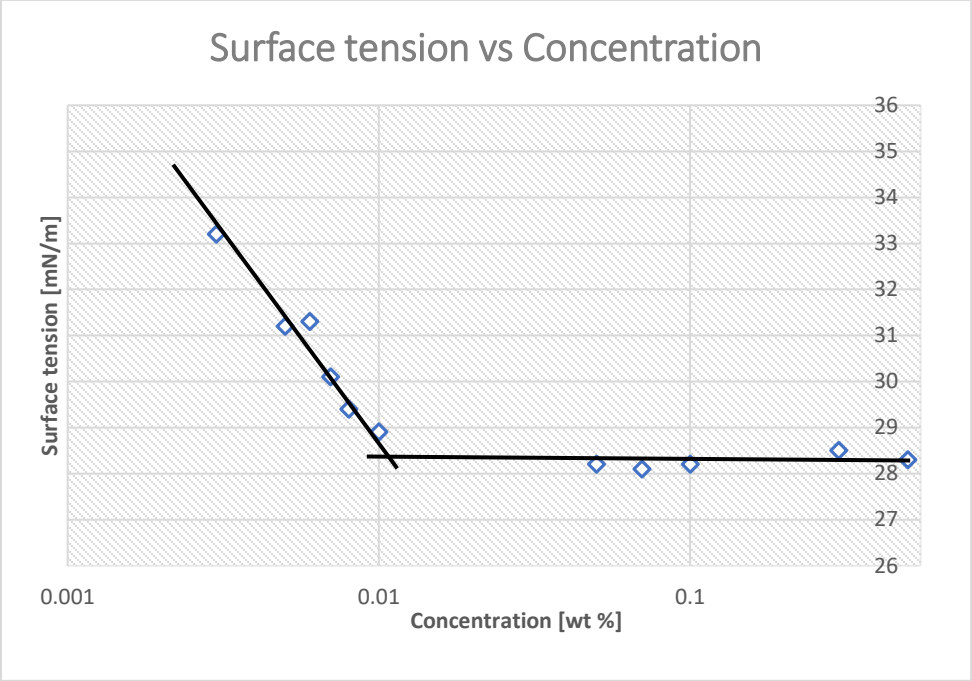

Figure E.2: CMC determination for APG surfactant solution

The CMC of the APG surfactant in 1 wt.% NaCl solution was determined to be 0.01 wt %.

F. Berea core minerology

A minerology study on Berea sandstone was carried out using the BASICA® application to quantify the amount of clays and heavy metals in the core. The results are presented in Table F.1 below;

Table F.1: A summary of the mineralogy of Berea core.

	MOLE AMOUNT	MOLE %
RUTILE	0.85	0.62
Ca-APATITE	3.38E-02	0.02
GYPSUM	3.50E-02	0.03
DOLOMITE	0.78	0.56
CHlORITE	0.17	0.12
HEMATITE	0.45	0.32
HALITE	7.04E-02	0.05
ALBITE	0.53	0.38
ILLITE	3.57	2.58
KAOLINITE	1.94	1.40
QUARTZ	129.99	93.90
TOTAL	138.43	100

The Berea core was found to consist of at least 4.01 mole% clays (shown in blue).

G. Flow rate determination

The following constants shown in Table G.1 and formulae were used to calculate the flow rates for the surfactant solution, gas and oil for this study.

Table G.1: Relevant constants for flow rate determination

Constants	Values
MW_o [g/mol]	142.29
MW_g [g/mol]	44.01
ρ_o [g/cm3]	0.722
ρ_w @ 20deg [g/cm3]	1.05
ρ_w@ 40deg [g/cm3]	1.02

Where MW is the molecular weight

- ρ is the density

-C is the molar density ($\frac{\rho}{MW}$)

1) The flow fraction of CO_2-decane mixture be f_{mix} , the flow rate of the mixture is q_{mix} mL/min and the flow rate of the surfactant solution is q_w mL/min

$$f_g = \frac{q_{mix}}{q_{mix} + q_w} \quad \text{(G.1)}$$

If the molar fraction of CO_2 in the CO_2-decane mixture is XCO_2, and the total flow rate of surfactant and CO_2-decane mixture ($q_{mix} + q_{water}$) is q_{total} (mL/min),

2) The flow rate of surfactant solution at 40° will be (assuming total flow rate is also measured at 40°(in oven);

$$q_{water} = q_{total} \times (1 - f_{mix}) \quad \text{(G.2)}$$

The flow rate is assumed to be the value at 20°

3) The flow rate of the mixture at 40° will be;

$$q_{mix} = q_{total} \times f_{mix} \quad \text{(G.3)}$$

4) The density of the mixture is a function of Pressure and temperature. The densities at 90 bar and 40° were obtained from REFPROP [16].

5) The molecular weight of the mixture can be obtained by;

$$\mathrm{MW_{mix}} = (1 - \mathrm{XCO_2}) \times \mathrm{MW_o} + \mathrm{XCO_2} \times \mathrm{MW_g} \quad \text{(G.4)}$$

6) The molar density C at 40 and 20° can now be calculated from;

$$\mathrm{C} = (\frac{\rho}{\mathrm{MW}}) \quad \text{(G.5)}$$

Units derivation; $\frac{[\frac{\mathrm{g}}{\mathrm{cm^3}}]}{[\frac{\mathrm{g}}{\mathrm{mol}}]} = \frac{[\frac{\mathrm{g}}{\mathrm{mL}}]}{[\frac{\mathrm{g}}{\mathrm{mol}}]} = \left[\frac{\mathrm{mol}}{\mathrm{mL}}\right]$

7) The molar flow rate of the mixture at 40°C is;

$$\mathrm{q_{mol,mix}} = \mathrm{C_{mix}} \times \mathrm{q_{mix}} \quad \text{(G.6)}$$

Units derivation= $\left[\frac{\mathrm{mol}}{\mathrm{mL}} \times \frac{\mathrm{mL}}{\mathrm{min}}\right] = \left[\frac{\mathrm{mol}}{\mathrm{min}}\right]$

Note that C_{mix} is at 40°C (density at 40°C)

8) The molar flow rate of the oil is;

$$\mathrm{q_{mol,oil}} = \mathrm{q_{mol,mix}} \times (1 - \mathrm{XCO_2}) \quad \text{(G.7)}$$

It is assumed that decane is incompressible and its density remains the same at 20°C and at 40°C degrees. Therefore, the molar densities and flow rates will be the same.

9) The molar flow rate of CO_2 at 40° is;

$$\mathrm{q_{mol,gas}} = \mathrm{q_{mol,mix}} \times \mathrm{XCO_2} \quad \text{(G.8)}$$

10)The volume flow rate of oil at 20° and 40° is therefore;

$$q_{oil} = \frac{q_{mol,oil}}{C_{oil}} \quad \text{(G.9)}$$

Units derivation; $\left[\frac{\frac{mol}{min}}{\frac{mol}{mL}}\right] = \left[\frac{mL}{min}\right]$

11) The volume flow rate of CO_2 at 40° is therefore;

$$q_{gas} = \frac{q_{mol,gas}}{C_{gas}} \quad \text{(G.10)}$$

[mL/min]

The volume flow rate was converted to 20°by;

$$q_{gas}@20° = q_{gas}@40 \times \frac{\rho_{gas}@40°}{\rho_{gas}@20°} \quad \text{(G.11)}$$

H. Error Treatment

The error bars presented in the figures correspond to the standard deviation of the measurement signal. Only the fluctuations of pressure drop are considered:

$$\delta(\Delta P) = \sigma_{\Delta P} = \sqrt{\frac{1}{N-1}\sum_{i=1}^{N}(\Delta P_i - \overline{\Delta P})^2} \tag{H.2}$$

where ΔP_i is the i^{th} pressure drop sample, N is the number of samples in the pressure drop signal, and $\overline{\Delta P}$ is the arithmetic average of pressure drop samples:

$$\overline{\Delta P} = \sum_{i=1}^{N}\frac{\Delta P_i}{N} \tag{H.2}$$

The propagation of the pressure drop error to the apparent viscosity is calculated as:

$$\delta\mu_{app} = \left|\frac{\partial\mu_{app}}{\partial\Delta P}\right|\delta(\Delta P) = \left|\frac{kA}{QL}\right|\delta(\Delta P) \tag{H.3}$$

The sampling time step of pressure drop is 5 seconds.

Nomenclature

C_a: Capillary number [-]

f: foam quality, [-]

f_g^*: critical foam quality [-]

P_c^*: limiting capillary pressure, [Pa]

f_{mix}: gas-oil mixture fractional flow [-]

f_{gas}: gas fractional flow [-]

f_{oil}: mixture fractional flow [-]

q_{total}: total volumetric flow rate [cm^3/min]

q_{gas}: gas volumetric flow rate [cm^3/min]

q_{oil}: oil volumetric flow rate [cm^3/min]

q_{water}: surfactant volumetric flow rate [cm^3/min]

q_{mix}: volumetric flow rate of CO_2-decane mixture [cm^3/min]

$q_{mol,oil}$: molar flow rate of oil [mol/min]

$q_{mol,gas}$: molar flow rate of CO_2 [mol/min]

$q_{mol,mix}$: molar flow rate of CO_2-decane mixture [mol/min]

C_{mix}: molar density of the CO_2-decane mixture [mol/ml]

C_{gas}: molar density of CO_2 [mol/ml]

C_{oil}: molar density of oil [mol/ml]

ρ_{oil}: density of oil [kg/m3]

ρ_{gas}: density of gas[kg/m3]

ρ_{water}: density of water [kg/m3]

ρ_{mix}: density of CO_2-decane mixture [kg/m3]

MW_g: molecular weight of gas, [kg/mol];

MW_o: molecular weight of oil, [kg/mol];

μ_c: effective viscosity of continuous phase [Pa.s]

μ_{mix}: viscosity of CO_2-decane mixture [Pa.s]

σ_{ow}: interfacial tension between oil and water, [N/m]

σ_{wg}: interfacial tension between gas and water, [N/m]

μ_{app}: apparent viscosity [cP]

k: permeability [D]

u_{total}: total velocity [m/s]

∇P: Pressure gradient [bar/m]

ΔP: Pressure drop [bar]

φ: porosity [-]

L: Core length, [cm];

L_{in}: length of the inlet-section of the core [cm];

L_{mid}: length of the middle-section of the core [cm];

L_{out}: length of the outlet-section of the core [cm];

D: diameter of the core [cm]

PV: pore volume [cm^3]

T: temperature [°C];

P: pressure, [bar];

XCO_2: molar fraction of CO_2 in CO_2-decane mixture, [-]

K: power law coefficient [-]

n: flow behaviour index [-]

γ: shear rate [s^{-1}]

CMC: critical micelle concentration, [-]

Bibliography

[1] S. Kahrobaei, K. Li, S. Vincent-Bonnieu and R. Farajzadeh, “Effects of compositional variations on CO2 foam under miscible conditions.,” 2017.

[2] L. Romero-Zerón, Advances in Enhanced Oil Recovery Processes, Introduction to Enhanced Oil Recovery (EOR) Processes and Bioremediation of Oil-Contaminated Sites, InTech Europe, 2012.

[3] S. . K. Masalmeh, “Impact of Capillary Forces on Residual Oil Saturation and Flooding Experiments for mixed to Oil-Wet Carbonate Reservoirs,” 2012.

[4] F. M. Llave, F. T. Chung, R. W. Louvier and D. A. Hudgins, “Gas Miscible Displacement. Foams for Mobility Control and Improvement in Gas Sweep Efficiency,” 1989.

[5] X. Chen, “CO2 Enhanced Oil Recovery and Storage in Reservoirs,” 2007.

[6] G. Homsy, “Viscous fingering in porous media.,” *Annu. Rev. Fluid Mech,* vol. 19, p. 271–311, 1987.

[7] J. Waggoner, J. Castillo and L. Lake, “Simulation of EOR processes in stochastically generated permeable media.,” *SPE Formation Eval. 7,* p. 173–180, 1992.

[8] E. Claridge, “ Prediction of recovery in unstable miscible flooding.,” *SPE J. 12,* p. 143–155, 1972.

[9] K. S. Pedersen and P. Christensen, Phase behaviour of Petroleum Fluids, Taylor & Francis, 2006.

[10] M. R. Rasaei, M. Sahimi and M. Haghighi, “Gas Injection and Fingering In Porous Media,” 2006.

[11] W. . F. Yellig and R. . S. Metcalfe, “Determination and Prediction of CO2 Minimum Miscibility Pressures,” *Journal of Petroleum Technology,* 1980.

[12] D. Denney, “CO2-EOR Mobility and Conformance Control: 40 Years of Research and Pilot Tests,” *Journal of Petroleum Technology,* 2013.

[13] B. Liu, J. Shi, J. Zhang, B. Sun and Y. Shen, “Reduction in interfacial tension of water-oil interface by supercritical CO2 in enhanced oil recovery processes studied with molecular dynamics simulation,” *The journal of supercritical Fluids 111,* pp. 171-178, 2016.

[14] C.-Y. Sun and G.-J. Chen, “Measurement of Interfacial Tension for the CO2 Injected Crude Oil + Reservoir Water System,” *Journal of Chemical & engineering data 50,* pp. 936-938, 2005.

[15] A. Georgiadis, F. Llovell, A. Bismarck, F. J. Blas, A. Galindo, G. C. Maitland, J. M. Trusler and G. Jackson, “Interfacial tension measurements and modelling of (carbon dioxide + n-alkane) and (carbon dioxide + water) binary mixtures at elevated pressures and temperatures,” *The Journal of Supercritical fluids 55,* pp. 743-754, 2010.

[16] E. W. Lemmon, M. L. Huber and M. O. McLinden, *Reference fluid thermodynamic and transport properties–REFPROP Version 8.0,* NIST standard reference database 23, 2007.

[17] D. D. Joseph, “Understanding foams and foaming,” *Journal of Fluids Engineering,* 1997.

[18] R. Taylor, “The Art and Science of Foam Bubbles,” *Nonlinear Dynamics, Psychology, and Life Sciences,* vol. 15, no. 1, pp. 129-136, 2011.

[19] M. I. Al-Mossawy, B. Demiral and D. M. Anwar Rajar, “Foam dynamics in porous media and its applications in Enhanced oil recovery,” 2011.

[20] D. Meyers, Surfactant Science and Technology 3rd Edition, John Wiley & Sons Inc, 2006.

[21] J. L. Salager, Surfactants: Types and Uses, 2002.

[22] A. J. J. O'Lenick, L. Siltech and K. O’Lenick, Effect of Branching on Surfactant Properties of Sulfosuccinates, 2007.

[23] O. Rangel-Yagui, A. Pessoa Junior and C. Tavares, “Micellar solubilization of drugs,” *J Pharm Pharmaceut Sci,* vol. 8, no. 2, pp. 147-163, 2005.

[24] P. Atkins and J. d. Paula, Atkins' Physical Chemistry, 2010.

[25] O. s. Owete and W. E. Brigham, “ Flow Behavior of Foam: A Porous Micromodel Study.,” 1987.

[26] R. K. Prud'homme, Foams: Theory: Measurements: Applications, 1995.

[27] S. S. Adkins, X. Chen, Q. . P. Nguyen, A. W. Sanders and . K. . P. Johnston, “Effect of branching on the interfacial properties of nonionic hydrocarbon surfactants at the air–water and carbon dioxide–water interfaces,” *Journal of Colloid and Interface Science 346,* p. 455–463, 2010.

[28] R. Varadaraj, J. Bock, S. Zushma, N. Brons and J. T. Colletti, *J. Colloid Interface Sci 147,* p. 387, 1991.

[29] H. Schott , “Foaming of Nonionic Surfactant Solutions: Effect of Surfactant Concentration and Temperature,” *Journal of the American Oil Chemists Society,* vol. 65, no. 5, p. 816–819, 1988.

[30] Z. F. Zhang, V. L. Freedman and L. Zhong, “Foam transport in porous media- A review,” 2009.

[31] S. H. Yang and R. L. Reed, “Mobility Control Using C02 Foams,” Society of Petroleum Engineers, 1989.

[32] M. Chen and Y. C. Yortsos, “Pore-network study of the mechanisms of foam generation in porous media,” Physical Review E, 73, 036304., 2006.

[33] K. Ma, C. A. Miller, S. L. Biswal, G. J. Hirasaki, J. L. Lopez-Salinas and M. C. Puerto, “Estimation of Parameters for the Simulation of Foam Flow through Porous Media. Part 1: The Dry-Out Effect,” *Energy & Fuels 2013 DOI: 10.1021/ef302036s,* p. 2363−2375, 2013.

[34] P. Gauglitz, F. Friedmann and S. Kam, “Foam Generation in Porous Media,” in *SPE/DOE Improved Oil Recovery Symposium*, 2002.

[35] D. Espinosa, F. Calderas, K. Johnston, S. L. Bryant and C. Huh, “Nanoparticle-stabilized supercritical CO2 foams for potential mobility control applications,” Society of Petroleum Engineers, 2010.

[36] R. F. Li, W. Yan, S. Liu, G. J. Hirasaki and C. A. Miller, “Foam Mobility Control for Surfactant enhanced oil Recovery,” 2008.

[37] S. I. Chou, “Conditions for generating foam in porous media.,” Society of Petroleum Engineers, 1991.

[38] R. Farajzadeh, A. Andrianov, R. Krastev, G. Hirasaki and W. Rossen, “Foam-Oil Interaction in Porous Media: Implications for Foam Assisted Enhanced Oil Recovery,” *Advances in Colloid and Interface Science 183–184,* pp. 1-13, 2012.

[39] A. H. Falls, G. J. Hirasaki, T. W. Patzek, D. A. Gauglitz, D. D. Miller and T. Ratulowski, “Development of a Mechanistic Foam Simulator: The Population Balance and Generation by Snap_off,” 1988.

[40] D. Weaire and S. Hutzler, “The physics of foams,” Oxford University Press, New York, 1999.

[41] K. Osei-Bonsu, N. Shokria and P. Grassiab, “Foam stability in the presence and absence of hydrocarbons: From bubble- to bulk-scale,” *Colloids and Surfaces A: Physicochemical and Engineering Aspects Vol 481,* p. Pages 514–526, 2015.

[42] L. Wang and R.-H. Yoon, “Stability of foams and froths in the presence of ionic and non-ionic surfactants,” *Minerals Engineering 19,* p. 539–547, 2005.

[43] F. Brasz, “Soap Films: Statics and Dynamics,” 2010.

[44] W. Liguang and Y. Roe-Hoan, “Effects of surface forces and film elasticity on foam stability,” 2008.

[45] R. Farajzadeh, A. Andrianov, H. Bruining and P. L. Zitha, “Comparative Study of CO2 and N2 Foams in Porous Media at Low and High Pressure-Temperatures,” 2009.

[46] F. G. Gandolfo and H. L. Rosano, “Interbubble Gas Diffusion and the Stability of Foams,” *Journal of colloid and interface science 194,* p. 31–36, 1997.

[47] L. E. Nonnekes, W. R. Rossen and S. J. Cox, “Effect of Gas Diffusion on Mobility of Foam for Enhanced Oil Recovery,” *Transport in Porous Media,* vol. 106, no. 3, pp. 669-689, 2015.

[48] M. Simjooa, T. Rezaei, A. Andrianov and P. Zitha, “Foam stability in the presence of oil: Effect of surfactant concentration and oil type,” *Colloids and Surfaces A: Physicochem. Eng. Aspects 438,* pp. 148-158, 2013.

[49] K. Koczo, L. A. Lobo and D. T. Wasan, Effect of Oil on Foam Stability: Aqueous Foams Stabilized by Emulsions, 1991.

[50] K. Teerakijpaiboon and F. Srisuriyachai, “The Effect of Foam Stability in CO2-Foam Flooding,” in *The 11th international Conference on Mining, materials and Petroleum Engineering*, Chiang Mai, Thailand, 2013.

[51] K. Osei-Bonsu, P. Grassia and N. Shokri, “Investigation of foam flow in a 3D printed porous medium in the presence of oil,” *Journal of Colloid and Interface Science 490,* pp. 850-858, 2016.

[52] D. T. Wasan, A. D. Nikolov, D. D. W. Huang and D. A. Edwards, *"Surfactant Based Mobility Control",* Michigan, 1987.

[53] L. L. Schramm, “Emulsions: Fundamentals & Applications in the Petroleum Industry,” *Advances in Chemistry, 231,* pp. 131-170, 1992.

[54] J. Lee, A. Nikolov and D. Wasan, “Surfactant micelles containing solubilized oil decrease foam film thickness stability,” *Journal of Colloid and Interface Science,* pp. 18-25, 2014.

[55] X. Xu, A. Saeedi and K. Liu, “Experimental Study on a Novel Foaming Formula for CO2 Foam Flooding,” *Journal of Energy Resources Technology, DOI: 10.1115/1.4034069,* 2016.

[56] S. A. Jones, G. Laskaris, S. Vincent-Bonnieu, R. Farajzadeh and W. R. Rossen, “Effect of surfactant concentration on foam: From coreflood experiments to implicit-texture foam-model parameters,” *Journal of Industrial and Engineering Chemistry 37 (2016) ,* p. 268–276, 2016.

[57] K. G. Kornev, A. V. Neimark and A. N. Rozhkov, “Foam in porous media: thermodynamic and hydrodynamic peculiarities,” *Advances in Colloid and Interface Science,* pp. 127-187, 1999.

[58] A. Ocampo, A. Restrepo, H. Cifuentes, J. Hester, N. Orozco, C. Gil, E. E. Ltd, SPE, S. Lopera, C. Gonzalez and U. N. D. Colombia, “Successful Foam EOR Pilot in a Mature Volatile Oil Reservoir Under Miscible Gas Injection,” 2013.

[59] T. Blaker, M. G. Aarra, A. Skauge, L. Rasmussen, H. K. Cellus, H. A. Martinsen and F. Vassenden, “Foam for Gas Mobility COntrol in the Snorre Field: THe FAWAG project,” Society of Petroleum Engineers, 2002.

[60] F. Martin, J. Stevens and K. Harpole, “CO2-Foam Field Test at the East Vacuum Grayburg/San Andres Unit,” SPE, 1994.

[61] A. W. Sanders, R. M. Jones, M. Linroth and Q. P. Nguyen, “Implementation of a CO2 foam Pilot Study in the SACROC field: Performance Evaluation,” 2012.

[62] J. Mukherjee, Q. P. Nguyen, J. Scherlin, P. Vanderwal and P. Rozowski, “CO2 Foam Pilot in Salt Creek, Natrona COunty, WY: Phase III: Analysis of Pilot Performance,” SPE, 2016.

[63] S. Chou, S. Vasicek, D. Pisio, D. Jasek and J. Goodgame, “CO2 Foam Field Trial at North Ward-Estes,” SPE, 1992.

[64] M. I. Romero, “Flow of emulsions in porous media,” 2009.

[65] C. D. McAuliffe, “Oil-in-Water Emulsions and Their Flow Properties in Porous Media,” Society of Petroleum Engineers, 1973.

[66] M. I. Romero, “Flow of emulsions in Porous Media,” 2009.

[67] H. Soot and C. J. Radke, “A filtration model for the flow of dilute stable emulsions in porous media,” 1984.

[68] S. Cobos, M. S. Carvalho and V. Alvadro, “Flow of oil–water emulsions through a constricted capillary,” *International Journal of Multiphase Flow 35 ,* p. 507–515, 2009.

[69] S. Buret, L. Nabzar and A. Jada, “Emulsion deposition in Porous media: Impact on well Injectivity,” Society of Petroleum engineers, 2008.

[70] A. C. Uzoigwe and S. S. Marsden Jr, “Emulsion rheology and flow through Unconsolidated Synthetic Porous media,” American Institute of Mining, metallurgical, and Petroleum Engineers, Dallas, 1970.

[71] H. O. Lee, J. P. Heller and A. M. W. Hoefer, “Change in Apparent Viscosity of CO2 Foam With Rock Permeability.,” Society of Petroleum Engineers. , 1991.

[72] M. Parlar, M. D. Parris, R. J. Jasinski and J. A. Robert, “An Experimental Study of Foam Flow Through Berea Sandstone With Applications to Foam Diversion in Matrix Acidizing.,” Society of Petroleum Engineers, 1995.

[73] R. Pal and E. Rhodes, “Viscosity/Concentration Relationships for Emulsions,” *Journal of Rheology,* vol. 33, no. 7, 1989.

[74] T. F. Tadros, “Emulsion Formation, Stability, and Rheology,” 2013.

[75] D.-X. Du, A. N. Beni, R. Farajzadeh and P. L. J. Zitha, “Effect of Water Solubility on Carbon Dioxide Foam Flow in Porous Media: An X-ray Computed Tomography Study,” *Industrial & Engineering Chemistry Research,* vol. 47, no. 16, pp. 6298-6306, 2008.

[76] R. Farajzadeh, R. M. Muruganathan, W. R. Rossen and R. Krastev, “Effect of gas type on foam film permeability and its implications for foam flow in porous media.,” *Advances in colloid and interface science,* vol. 168, no. 1, pp. 71-78, 2011.

[77] P. Q. Nguyen, *Dynamics of foam in porous media,* 2004.

[78] A. F. Morais, H. Seybold, H. J. Herrmann and J. S. Andrade Jr, “Non-Newtonian fluid flow through three-dimensional disordered porous media.,” *Physical review letters,* vol. 103, no. 19, p. 194502, 2009.

[79] T. Sochi, “Flow of Non-Newtonian Fluids in Porous Media,” *Journal of Polymer Science,* vol. 48, no. 23, pp. 2437-2767, 2010.

[80] F. Friedmann and J. A. Jensen, “Some Parameters Influencing the Formation and Propagation of Foams in Porous Media.,” Society of Petroleum Engineers, 1986.

[81] S. Siddiqui, S. Talabani, S.T.Saleh and M. Islam, “Foam flow in low-permeability Berea Sandstone cores: a laboratory investigation,” *Journal of Petroleum Science and Engineering,* vol. 36, no. 3-4, pp. 133-148, 2002.

[82] Y. T. Oikawa and T. T, “Effect of CO2 injection on mechanical properties of berea sandstone.,” in *The 42nd US Rock Mechanics Symposium (USRMS)*, 2008.

[83] J. P. Kaszuba, D. R. Janecky and M. G. Snow, “Experimental evaluation of mixed fluid reactions between supercritical carbon dioxide and NaCl brine: Relevance to the integrity of a geologic carbon repository.,” *Chemical Geology,* vol. 217, no. 3, pp. 277-293, 2005.

[84] S. Iglauer, M. Sarmadivaleh, A. Al-Yaseri and M. Lebedev, “Permeability evolution in sandstone due to injection of CO2-saturated brine or supercritical CO2 at reservoir conditions.,” *Energy Procedia,* vol. 63, pp. 3051-3059, 2014.

[85] I. M. Mohamed, J. He and H. A. Nasr-El-Din, “Carbon Dioxide Sequestration in Sandstone Aquifers: How Does It Affect the Permeability?,” in *Carbon Management Technology Conference*, 2012.

[86] J. Kim, Y. Dong and W. R. Rossen, “Steady-State Flow Behavior of CO2 Foam,” Society of Petroleum Engineers., 2005.

[87] S. F. Kia, H. S. Fogler and M. G. Reed, “Effect of Salt Composition on Clay Release in Berea Sandstones.,” Society of Petroleum Engineers., 1987.

[88] Z. Duan and S. Rui, “An improved model calculating CO2 solubility in pure water and aqueous NaCl solutions from 273 to 533 K and from 0 to 2000 bar.,” *Chemical geology,* vol. 193, no. 3, pp. 257-271, 2003.

[89] S. T. Hangx, “Behaviour of the CO2-H2O system and preliminary mineralisation model and experiments,” CATO Workpackage WP, 2005.

[90] A. Muggeridge, . A. Cockin, K. Webb, H. Frampton, I. Collins, T. Moulds and P. Salino, “Recovery rates, enhanced oil recovery and technological limits,” 2013.

[91] G. Khan, “Experimental studies of Carbon dioxide Injection for enhanced Oil,” Master Thesis Aalborg University Esbjerg, Esbjerg, 2009.

[92] A. Mazzoldi, D. Picard, P. Sriram and C. Oldenburg, “Erratum to ‘Simulation-based estimates of safety distances for pipeline transportation of carbon dioxide’,” *Greenhouse Gases: Science and Technology 3(2):1-18,* pp. 3(2):1-18, 2013.

[93] J. A. Heuser, A. R. Taulbee, W. U. Spendel, M. R. Hughes and G. E. Pacey, “Foam Drainage Investigated Using Terahertz Spectroscopy,” 2008.

[94] P. Held, “Rapid Critical Micelle Concentration (CMC) Determination Using Fluorescence Polarization,” 2014.

[95] A. R. Kovsek and H. J. Bertin, “Estimation of Foam Mobility in Heterogeneous Porous Media,” Society of Petroleum engineers, 2002.

[96] S. Eva, F. Ravera, M. Ferrari, C. Stubenrauch, A. Makievski and J. Kragel, “A surface rheological study of non-ionic surfactants at the water–air interface and the stability of the corresponding thin foam films,” vol. 298, 2006.

[97] R. Chanamai and D. J. McClements, “Dependence of creaming and rheology of monodisperse oil-in-water emulsions on droplet size and concentration,” *A: Physicochemical and Engineering Aspects 172,* pp. 79-86, 2000.

[98] P. A. Gauglitz, F. Fiedmann, S. I. Kam and W. R. Rossen, “Foam generation in homogeneous porous media,” *Chemical Engineering Science,* vol. 57, pp. 4037-4052, 2002.

[99] D. Amiel and M. J. S. Sullivan, “The Rheology of Foam,” in *Fall Meeting of the Society of Petroleum Engineers of AIME*, 1969.

Acknowledgements

The last ten months have taught me more about myself than any other academic experience in my life. I will always cherish this experience and will always be grateful to the people without whose support I would not be where I am today.

I would like to thank Dr. Rouhi Farajzadeh for his guidance during the course of this thesis. I would also like to thank Dr. Sebastien Vincent Bonnieu and Dr. Siavash Kahrobaei for the useful discussions and comments on my thesis.

I would like to acknowledge the Dietz Lab of Delft University of Technology where all the experiments were carried out and I'm also thankful for the technical support availed to me by Michiel Slob.

I would like to acknowledge the Justus and Louise foundation for the funding provided to me through the Justus and Louise academic excellence scholarship.

Lastly, I would like to thank my parents for their unwavering support throughout this Master's program.

Rita Bagaine Kagoro

TU Delft